

## Recent advances in geostationary satellites for inland and coastal aquatic systems: scientific research and applications

Carina F. Portela, Vitor S. Martins, Evlyn M. L. M. Novo, Rejane S. Paulino & Cláudio C. F. Barbosa

**To cite this article:** Carina F. Portela, Vitor S. Martins, Evlyn M. L. M. Novo, Rejane S. Paulino & Cláudio C. F. Barbosa (2024) Recent advances in geostationary satellites for inland and coastal aquatic systems: scientific research and applications, *International Journal of Remote Sensing*, 45:5, 1574-1607, DOI: [10.1080/01431161.2024.2314007](https://doi.org/10.1080/01431161.2024.2314007)

**To link to this article:** <https://doi.org/10.1080/01431161.2024.2314007>



View supplementary material [↗](#)



Published online: 15 Feb 2024.



Submit your article to this journal [↗](#)



Article views: 7



View related articles [↗](#)



View Crossmark data [↗](#)



## Recent advances in geostationary satellites for inland and coastal aquatic systems: scientific research and applications

Carina F. Portela<sup>a,b</sup>, Vitor S. Martins<sup>c</sup>, Evlyn M. L. M. Novo<sup>a,b</sup>, Rejane S. Paulino<sup>c</sup>  
and Cláudio C. F. Barbosa<sup>a,b</sup>

<sup>a</sup>Earth Observation and Geoinformatics Division (DIOTG), National Institute for Space Research (INPE), São José dos Campos, Brazil; <sup>b</sup>Instrumentation Laboratory for Aquatic Systems (LabISA), Earth Sciences General Coordination of the National Institute for Space Research (INPE), São José dos Campos, Brazil; <sup>c</sup>Department of Agricultural & Biological Engineering, Mississippi State University (MSU), Starkville, USA

### ABSTRACT

Inland and coastal environments are complex ecosystems composed of suspended and dissolved materials, affecting light propagation within the water column. Satellite-based water quality research relies on water optical properties provided by optical sensors on board of polar orbit satellites since the 1980's. Specifically, Geostationary (GEO) ocean colour satellites offer high temporal resolution (e.g. every 15-minute observations), moderate spatial resolution (0.5–1 km) at regional scale, making them a promising alternative to polar orbiting satellites for near-continuous monitoring of highly dynamic aquatic ecosystems. This literature review examines the evolution of geostationary satellite technology and its applications in monitoring inland and coastal waters. A summary of the most relevant studies using geostationary sensors is provided for key water quality indicators such as chlorophyll-a and algal organisms, total suspended solids, and turbidity. Also, geostationary missions were well-detailed, with their available sensors and characteristics. Although this research topic is still incipient, recent studies have demonstrated the potential of GEO multi-spectral observations in understanding sub-daily water quality patterns. Notably, most research studies have focused on Asia, suggesting unexplored opportunities globally. Advanced Himawari Imager (AHI) and Geostationary Ocean Colour Imager (GOCI) have been used to improve water quality estimates, and inherent challenges were documented, such as algorithm validation, limited spatial resolution, and high volume of images and auxiliary files to be managed. The opportunities for new studies range from algorithm development for atmospheric correction, cloud masking, and bidirectional reflectance corrections to inter-comparison with existing sun-synchronous satellites. Geostationary satellites are promising avenues for future research on near-continuous monitoring of inland and coastal water resources.

### ARTICLE HISTORY

Received 18 October 2023  
Accepted 28 January 2024

**CONTACT** Carina F. Portela ✉ [carina.portela@inpe.br](mailto:carina.portela@inpe.br) 📧 Earth Observation and Geoinformatics Division (DIOTG), National Institute for Space Research (INPE), São José dos Campos, São Paulo 12227-010, Brazil

📄 Supplemental data for this article can be accessed online at <https://doi.org/10.1080/01431161.2024.2314007>

© 2024 Informa UK Limited, trading as Taylor & Francis Group

## 1. Introduction

Inland and coastal environments are optically complex ecosystems that typically have a mixture of suspended and dissolved organic and inorganic materials called Optically Active Constituents (OACs). When sunlight penetrates natural waters, the OACs (Sagan et al. 2020) are responsible for its absorption, refraction, and scattering (Kirk 2010) within the water column. These interactions, which vary according to the type and nature of each constituent, are quantified through inherent optical properties (IOP) and apparent optical properties (AOP) (IOCCG 2006; Preisendorfer 1976; Zaneveld and Ronald 2013). OACs include the pure water, the phytoplankton pigments such as chlorophyll-a (chl-a), non-algal particles, and coloured dissolved organic matter (CDOM) (IOCCG 2018). Satellite-based water quality research relies on analysing optical properties recorded by optical sensors, and for the past four decades, multi-spectral satellites sensors have been employed for this purpose (Aranha et al. 2022; Brezonik, Menken, and Bauer 2005; S.; S. Chen et al. 2015; Gholizadeh, Melesse, and Reddi 2016; Giardino et al. 2001; Guan et al. 2020; Letelier and Abbott 1996; Lima et al. 2023; Martins et al. 2019; Pahlevan et al. 2020; Ritchie, Cooper, and Schiebe 1990). Unlike conventional sampling points approaches, remote sensing data present a practical and affordable option for assessing water quality via bio-optical models (Duan et al. 2010; Hadjimitsis and Clayton 2009; Uudeberg et al. 2020; F. Zhang et al. 2021), which are essential for accurately detect environmental stresses (Ogashawara, Mishra, and Anatoly 2017). Since the launch of the Nimbus-7 spacecraft in 1978 having on board the Coastal Zone Color Scanner (CZCS), sun-synchronous satellites have been widely used for monitoring coastal and oceanic waters. Sun-synchronous orbit aligns with the average rate of Earth's rotation around the Sun, and it ensures a consistent passage over the equator at nearly the same local mean solar time throughout the year (Paek et al. 2020), which is critical for reliable solar illumination in remote sensing applications. Nevertheless, the temporal resolution of this type of orbit limits the monitoring short-term events, mainly in cloudy regions like the tropics (Neukermans, Ruddick, and Greenwood 2012).

Geostationary satellites maintain a constant observation relative to a specific point of the Earth's surface because the orbital period matches the Earth's rotation period of 24 hours, and they are typically positioned in a circular orbit directly above the Earth's equator at high altitude (>35,000 kilometres) (Soop 1994). These satellites are the most viable alternative for highly frequent observations from a fixed viewpoint in space, covering large swath areas for regional and global ocean colour studies. Geostationary satellites (GEO) have a high temporal resolution (e.g. 5–15-minute interval of ABI/GOES-16), a large imaging area with multispectral bands from visible to mid-infrared. Moreover, GEO satellites have the potential to capture a greater number of cloud-free pixels per day when compared to sun-synchronous satellites due to multiple observations of the same area daily. The high temporal resolution also enhances the opportunities for scientific studies about complex and dynamic natural events, providing near real-time observations for mapping and monitoring. Challenges associated with its orbit include limited coverage of high latitudes (>75 degrees), variability in sun-view geometry along the day that is still a challenge to overcome, and different optical paths for the reflected radiance from the surface to reach the satellite sensor. However, recent advances in image processing and radiative transfer calculations are gradually addressing these limitations in new

remote sensing products (e.g. Geostationary-NASA Earth Exchange), increasing their potential for studying dynamic aquatic systems (Dorji and Fearn 2018; K. Ruddick et al. 2014). Figure 1 presents examples of images captured by geostationary satellite sensors.

Historically, the first geosynchronous satellite (Syncom 3) launched in 1964 (Garriott, Smith, and Yuen 1965; Holtorf and Piccini 2009) aimed communication purposes. In the 1970's NASA and NOAA launched the first GOES (Geostationary Operational Environmental Satellite), followed by the METEOSAT (European Space Agency) and the Japanese Geostationary Meteorological Satellite (GMS). Traditionally, GEO missions aimed atmospheric studies and meteorologic modeling, with few studies exploring these images for inland and coastal monitoring. Until the early 2000s, the use of GEO for aquatic systems studies focused almost exclusively on the ocean environment, part of which related to ocean-atmosphere interaction and sea surface temperature (Apel 1980; Barrett and Hamilton 1982; Barton and Pearce 2006; Castelao et al. 2006; Chamberlin 1982; Darnell and Harriss 1983; Heta and Mitsuta 1993; Kazi 1990; Koffler 1975; Legeckis 1978; Legeckis and Zhu 1997; Legeckis, Brown, and Chang 2002; Legeckis, Pichel, and Nesterczuk 1983; Maturi et al. 2008; Maul et al. 1978; McClain 1980; Rajan et al. 2002). Davis and Abbott (2005) and Lomax et al. (2006) highlighted the role of GEO satellites for the observation of monitoring of coastal systems due to the frequency of data acquisition and their large coverage area. Those features opened a new research path for near-continuous observation system. More recently, NOAA's National Ocean Service created the nowCOAST, which incorporated GOES's visible and infrared images in an online mapping portal. This portal provides real-time coastal information for the United States, particularly valuable for monitoring cloud and storm events (Allard 2006). Studies based on GEO data application to inland and coastal water have become more frequent with the

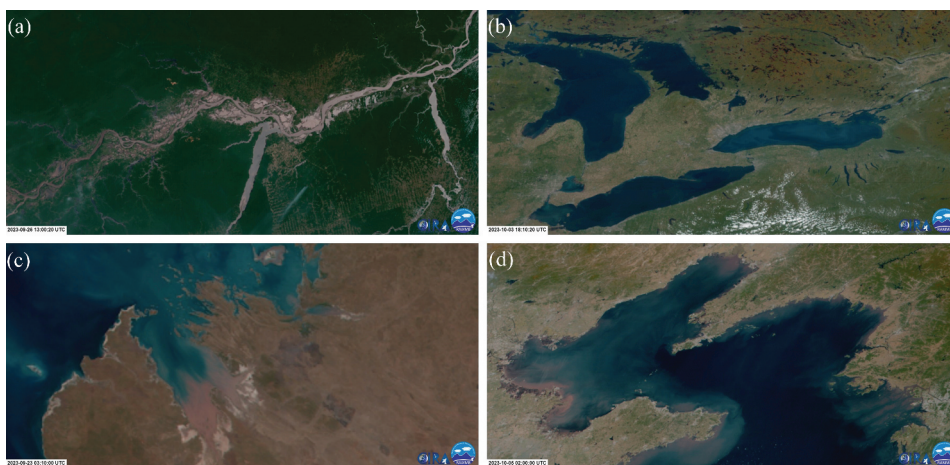


**Figure 1.** Examples of GEO images for inland and coastal waters: (a) Amazon River, Northern Brazil (2023-09-26, 13:00UTC), (b) lakes Huron, Erie and Ontario, US/Canada (2023-10-03, 18:10UTC); (c) Derby-West Kimberley Coast and Fitzroy River Estuary, Western Australia (2023-09-23, 03:10UTC); (d) Yellow Sea, China and Korean Peninsula (2023-10-05, 02:00UTC). All these images were made accessible by NOAA regional and mesoscale meteorology branch portal (<https://rammb-slider.cira.colostate.edu/>). Images a) and b) was captured by GOES-16/ABI sensor, and c) and d) by Himawari-9/AHI sensor.

improved payloads consisting of sensors suitable for monitoring aquatic ecosystems and ocean colour, such as GOCI and SEVIRI (Choi et al. 2012; IOCCG 2012; Jo, Yan, and Li 2010; Z. Lee et al. 2012; Neukermans et al. 2009b; K. Ruddick et al. 2012; Ryu et al. 2011; Son, Min, and Ryu 2012; M. Wang, Shi, and Jiang 2012).

Given the increasing application of GEO satellites for monitoring and analysing inland and coastal waters, this study aims to review the relevant literature on geostationary satellites and remote sensing focus on coastal and inland waters, organizes the available satellites sensors, research, and applications. Section 2 and 3 provides the definition and available satellites and multi-spectral sensors. Section 4 presents the GEO applications in the literature based on the water constituents (TSS, chl-a) and other applications. The contributions of this study are to support GEO applications and to provide an overview of the main studies for the scientific community in this field. This review consists of several publications from well-known remote sensing journals and a comprehensive search on WebOfScience using the keywords 'geostationary', 'coastal water', and 'inland water' and searching the title, abstract, keywords, and references from 2012 to 2020. The compilation of the last decade's studies shows that geostationary applications on coastal and inland waters are still incipient, but rapidly growing with the new multi-spectral sensors on board (see Figure 2). This study provides recent past, current, and potential contributions of geostationary satellites for near-continuous monitoring of large-scale water quality events in the aquatic environment.

## 2. Geostationary satellites

Satellite orbits can be classified according to altitude, eccentricity, and inclination (Capderou 2014). The most common orbits are the low polar, sun-synchronous, or

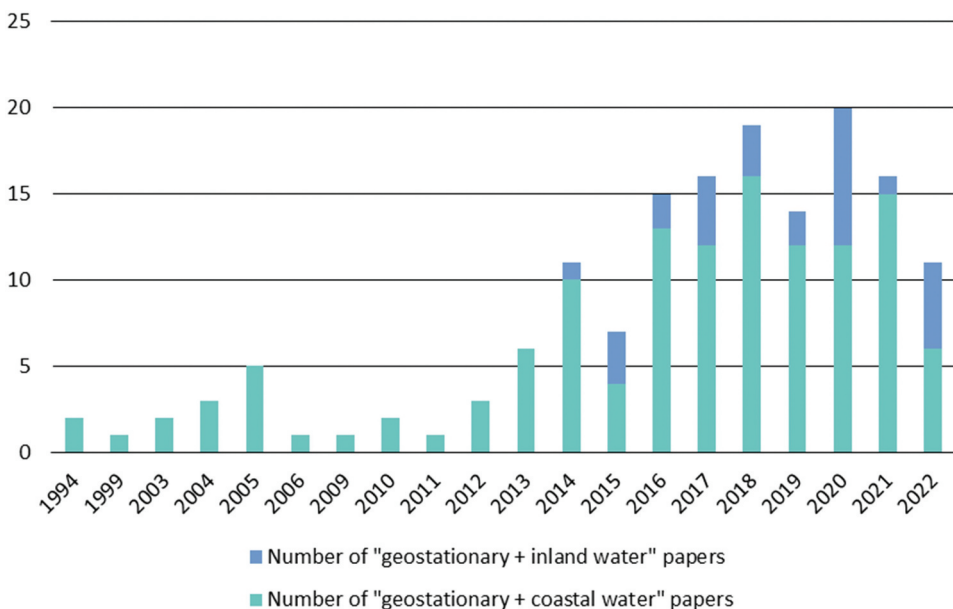


**Figure 2.** Number of papers published on geostationary satellites and inland and coastal water between 1994 and 2022.

not, and the geostationary. Polar orbits are low Earth orbits at altitudes from 200 to 1000 km. Satellites in sun-synchronous polar orbits usually travel over Earth from North to South, passing over Earth's poles. Sun-synchronous orbit is a particular kind of polar synchronized to keep its position relative to the Sun. That means the satellite observes a given point on the Earth daily. A satellite achieves the geostationary orbit at an altitude close to 35,000 km, remaining at a fixed longitude over the equator (Liang, Wang, and Jiang 2012). The paper 'Extra-terrestrial Relays' (Clarke 1945) was one of the first to mention geostationary orbit. The author proposed reliable radio communication worldwide based on three satellites positioned at 120° from each other in a specific orbit above the Earth's equator. This orbit allows the satellite to travel simultaneously to the Earth's rotation. After the first geostationary satellite launch in 1964, Syncom 3, hundreds of satellites have been launched into geostationary orbit, and applied to the most diverse fields of activities: communication, navigation, meteorology, and data transmission (H. Li 2014; Liang, Wang, and Jiang 2012). Over the years, scientific studies in different fields have been developed based on data provided by sensors coupled to geostationary satellites (Günthner et al. 2017; Hubert and Whitney 1971; Merchant et al. 2009; Tarpley 1979), applying methods for detecting solar radiation and irradiance (Jiang et al. 2019; Watanabe, Takenaka, and Nohara 2021; Yeom, Deo, et al. 2020), retrieving soil moisture (Ghilain et al. 2019; Y. Lee, Jung, and Kim 2019; Yan et al. 2022), detecting cloud cover (Yeom, Roujean, et al. 2020), and monitoring biomass burning, either based on direct estimates or through integrating data from polar satellite (F. Li et al. 2019; Mota and Wooster 2018; Pereira et al. 2022).

Appendix A summarizes Earth Observation Satellites currently in geostationary orbit (European Space Agency 2022; Union of Concerned Scientists 2022; World Meteorological Organization 2022). In general, image-type geostationary satellites have one spectral band with spatial resolution ranging from 250 m to 500 m, usually in the red or near-infrared region of the spectrum. Furthermore, most satellites were developed by Russia, China, South Korea, U.S.A., Japan, and India, with the addition of multinational missions linked to Europe. Most space missions were developed for meteorological purposes as their core application, but there are a large number of atmospheric studies, including air quality monitoring (Shu et al. 2022), surface air temperature (Z. Zhang and Du 2022), surface particles from dust events (Sowden, Mueller, and Blake 2018), and one example of detecting low strata and fog based on combined data from two geostationary satellites in the South Korea region (Yoo et al. 2018). Alternatively, geostationary satellite data has great potential for disaster risk management (Higuchi 2021). As data from geostationary satellites help study highly dynamic phenomena, the high temporal resolution makes them particularly useful for studying aquatic ecosystems, but new challenges associated with data processing, such as the improvement of atmospheric correction algorithms, bidirectional reflectance corrections, cloud masking, and spatial resolution limitations (K. Ruddick et al. 2014). Recent studies have been proposed to assess geostationary orbital systems (COMS-1, Himawari-8, and GOES-16) application to aquatic systems studies, including daily changes in surface temperature (Z. Huang and Feng 2021; Park, Woo, and Lee 2020), primary production in coastal regions (Asaoka et al. 2020), water turbidity (S. Wang et al. 2020), algae monitoring (Fu et al. 2021; Minghelli et al. 2021), among others. The following sections will better explore them through the recent studies in inland and coastal aquatic systems.



### 3. Current geostationary satellites for inland and coastal studies

Water colour retrieval depends on the solar irradiance spectrum, atmospheric conditions, solar and viewing geometries, and on the absorption and scattering properties of water and the substances that are dissolved or suspended in the water column, e.g. phytoplankton, CDOM (coloured dissolved organic matter), and suspended sediments (Mobley, 1994). The propagation of the radiation through the water column results in the interaction of photons with their different constituents and determines the spectral composition of the light emerging and the water colour perceived by the human eye (Pozdnyakov, Grassl, and Graßl 2003). Radiometric measurements translate the water colour into spectral variations in the water-leaving radiance, which is converted to remote sensing reflectance from the ratio of water-leaving radiance by the downward irradiance above the water surface (Mobley 1999). The goal of the satellite ocean colour analysis is to accurately estimate the water-leaving radiance spectra to derive other geophysical and optical quantities from those spectra, e.g. the concentration of the photosynthetic pigment chlorophyll-a. The accurate water colour measurement depends on different parameters, such as the surface water's optical properties and the daylight's spectral distribution (Højerslev 1980). Achieving an accurate measurement of the water's inherent colour through remote sensing presents a significant challenge. In this way, there is a continuous effort to refine correction techniques for enhancing satellite data quality for water studies. These advancements include, among others, atmospheric correction (J.-H. Ahn et al. 2012; Dorji and Fearn 2018; Emberton et al. 2016; Ilori, Pahlevan, and Knudby 2019; Martins et al. 2017; Moses et al. 2017; Novoa et al. 2017; Song et al. 2023), glint correction (Bernardo et al. 2018; Kay, Hedley, and Lavender 2009; Kutser, Vahtmäe, and Praks 2009; Overstreet and Legleiter 2017; H. Zhang and Wang 2010) and adjacency effects (Bulgarelli and Zibordi 2018; Pan, Bélanger, and Huot 2022; Paulino et al. 2022; Santer and Schmechtig 2000; Wu, Knudby, and Lapen 2023). Figure 3 shows the location of current operational geostationary satellites relevant to the water colour studies. Except for GOCI II, selected GEO satellites sensors mentioned hereafter were not designed for water colour measurements in remote sensing, but these might be useful (Groom et al. 2019), and Section 4 presents their main applications.

#### 3.1. GEO-KOMPSAT-2B/GOCI-II

GEO-KOMPSAT-2B was successfully launched in February 2020, and is located at longitude 128.2° East; after about six months of in-orbit testing, it began its regular operation in October 2020 (M.-S. Lee, Park, and Micheli 2021). Since then, the Ocean Satellite Center of the Korea Institute of Ocean Science and Technology has received, processed, quality checked, stored, and distributed GOCI-II data, which is one of the sensors in GEO-KOMPSAT-2B, with a planned life span of 10 years. GOCI-II took over the mission of its predecessor GOCI, flown on COMS-1, featuring an improved spatial resolution of 250 m compared to GOCI's 500 m and 12 visible and near-infrared bands compared to the previous 8 bands (Choi et al. 2021; European Space Agency 2022; M.-S. Lee, Park, and Micheli 2021). The scientific community expects that GOCI-II will be widely used in various regions and subjects, such as efficient marine environment management, real-time nautical disaster monitoring, and provision of fisheries environment through ecological



**Figure 3.** Position of geostationary satellites with potential for inland and coastal waters studies.

environment analysis (Yong et al. 2021). GOCI-II has 13 channels: 1 band in the UV (ultraviolet), 8 bands in the visible light, 3 bands in the near-infrared (NIR); broad bandwidths between 0.360 and 0.900  $\mu\text{m}$ , and 0.010–0.040  $\mu\text{m}$ . The Signal-to-Noise Ratio (SNR) from the satellite sensor bands varies from 788 to 1228 (European Space Agency 2022).

### 3.2. GOES-16, 17, and 18/ABI

Geostationary Operational Environmental Satellite-R (GOES-R) Series is the NOAA's newest generation of meteorological geostationary satellites currently operated in a three-satellite system, including GOES-16, GOES-17, and GOES-18. GOES-16 was launched into a geostationary orbit in 2016 and became fully operational on 18 December 2017. The GOES-16 has its nadir location in Colombia (75.2°W 0.0°N) and senses a geographic area from West Africa to about 138°W over the Pacific Ocean, most of North and all of South America (Schmit et al. 2018; S. Wang et al. 2020). GOES-17, launched in March 2018, is located on the equator at 104.7° W (European Space Agency 2022; Z. Zhang and Du 2022). GOES-18 is the 3rd flight unit of the GOES 3rd generation program. Was launched in March of 2022 with longitude at GOES-WEST position 137°W to allow operational use of imagery during degraded GOES-17 imagery.

GOES-16, 17, and 18 carry onboard the Advanced Baseline Imager (ABI), with more spectral bands and four and five times finer spatial and temporal resolution, over legacy GOES sensors (Schmit et al. 2017). The ABI acquires multi-spectral observations every 10 min, formerly every 15 min, has ten thermal emissive bands from 3.90  $\mu\text{m}$  to 13.3  $\mu\text{m}$  and six reflective bands corresponding to the blue (1 km at nadir 0.45–0.49  $\mu\text{m}$ ), red (0.5 km at nadir 0.60–0.68  $\mu\text{m}$ ), NIR (1 km at nadir 0.847–0.882  $\mu\text{m}$ ), and three shortwave infrared (SWIR) (2 km at nadir 1.366–1.380  $\mu\text{m}$ , 1 km at nadir 1.59–1.63  $\mu\text{m}$ , and 2 km at nadir 2.22–2.27  $\mu\text{m}$ ) wavelength regions (Miller et al. 2012). The SNR from its visible, NIR, and SWIR bands is 300 with 100% albedo as input (European Space Agency 2022). The information from the ABI on the GOES-R series can support many applications related to severe weather, tropical cyclones



and hurricanes, aviation, natural hazards, land and ocean surfaces, climate dynamics, and the cryosphere, with an excellent temporal resolution from 60 s to 15 min (McCorkel et al. 2020).

### **3.3. Himawari-8 and 9/AHI**

Himawari-8, located at 140.7° E, with East/Southeast Asia and Oceania as its primary observation area. Himawari-8 is a geostationary meteorological satellite launched by JAXA (Japan Aerospace Exploration Agency) in October 2014. Now operated by JMA (Japan Meteorological Agency), it became operational in July 2015 (Bessho et al. 2016). Equipped with the Advanced Himawari Imager (AHI), which is comparable to the Advanced Baseline Imager (ABI) on board the U.S. GOES-R series satellites, it provides full-disk images of the Earth every 10 min at a spatial resolution of 0.02° (~2 km). AHI takes images from Japan every 2.5 min, and landmark area images every 0.5 min. These images can be used to identify and track rapidly changing weather patterns and derivate quantitative products (Bessho et al. 2016; X. Zhang et al. 2022).

The AHI has 16 bands: three visible bands centred at 0.455, 0.51, and 0.645  $\mu\text{m}$ ; one NIR band centred at 0.86, two SWIR 1.61, and 2.26  $\mu\text{m}$ ; and ten thermal infrared (TIR) bands centred at 3.85, 6.25, 6.95, 7.35, 8.6, 9.63, 10.45, 11.2, 12.35 and 13.3  $\mu\text{m}$ . The spatial resolutions of the visible band at 0.645  $\mu\text{m}$ , the other visible bands plus the NIR band, and all other SWIR and TIR bands are approximately 0.5, 1.0, and 2.0 km at the sub-satellite point, respectively (European Space Agency 2022; Murakami 2016). The SNR from its visible, NIR and SWIR bands is approximately equal or greater 300, with 100% albedo as input (European Space Agency 2022).

### **3.4. Fengyun 4A and 4B/AGRI**

China's FY-4 series of geostationary weather satellites are designed to enhance weather forecasting and services, and the key instruments on board include the Advanced Geostationary Radiation Imager (AGRI), Lighting Mapping Imager, Prototype Geostationary Interferometric Infrared Sounder, and Space Environment Package (Yang et al. 2017). These satellite sensors produce various products such as atmospheric profiles, lightning distribution, and water vapour data. FY-4A, launched in December 2016 and located at 104.7° E, was an experimental satellite system, while FY-4B, launched in June 2021 at longitude 133° E, marked the operational phase. The FY-4 series forms a dual satellite network that frequently monitors atmospheric and terrestrial conditions, generating various meteorological parameters and products, including cloud top temperature analysis, detection of dust storms, and fire hot spots (J. Chen et al. 2023).

The AGRI performs accurate calibration and observation capabilities. It covers 15 spectral bands with varying spatial resolutions (1 km and 0.5 km for visible centred at 0.47 and 0.65  $\mu\text{m}$ , 1 km and 2 km for near-infrared centred at 0.825, 1.378, 1.61 and 2.25  $\mu\text{m}$ , and 4 km for infrared channels centred at 3.75, 6.25, 6.95, 7.1, 7.42, 8.55, 10.80, 12.00, 13.50  $\mu\text{m}$ ), observed at intervals of 15 minutes. The sensor's channels span multiple ranges, enabling cloud identification, earth temperature estimation, and carbon dioxide detection. The minimum SNR value varies between 90 and 200, with 100% albedo as input for the visible and NIR bands (European Space Agency 2022).

### 3.5. *Meteosat second Generation/SEVIRI*

Meteosat Second Generation (MSG) aimed to improve image quality compared to the first generation, allowing meteorologists to offer more accurate mid and short-term weather forecasts. Equipped with instruments such as the Spinning Enhanced Visible and Infrared Imager (SEVIRI) and the Geostationary Earth Radiation Budget (GERB), the MSG series' primary mission is to provide operational meteorology and climate monitoring data. MSG comprises four satellites in geostationary orbit, providing essential data for various fields dependent on meteorological phenomena, benefiting agriculture, oceanography, and hydrology. ESA launched Meteosat 8, 9, 10, and 11 satellites at specific orbits in 2002, 2005, 2012, and 2015, respectively, at longitudes 45.5° E, 0.0° and 9.5° E with operational objectives. Meteosat 8 is no longer operating.

The Spinning Enhanced Visible and Infrared Imager (SEVIRI) is the primary payload on the Meteosat Second Generation (MSG) satellite, with 12 spectral channels, including visible, near-infrared, and infrared wavelengths, with spatial resolutions ranging from 3 km to 1 km. Its 15-minute imaging cycle captures images of the Earth's disk, facilitating various applications such as solar modelling, agricultural studies, forest fire monitoring, and meteorological analysis. Despite its limitations in detecting ocean colour, SEVIRI's capabilities are valuable for climate monitoring. The SEVIRI spectral channels consist of three Visible and Near-Infrared (VNIR) channels (centred at 0.635, 0.81 and 1.64  $\mu\text{m}$ ), eight Infrared (I.R.) channels (centred at 3.92, 6.25, 7.35, 8.70, 9.66, 10.8, 12.0 and 13.4  $\mu\text{m}$ ) and one visible broadband channel (at 0.6–0.9  $\mu\text{m}$ ) called the High-Resolution Visible channel (HRV). Their SNR values vary between 3 and 10.1, with 1% albedo as input for the visible and NIR bands (European Space Agency 2022).

### 3.6. *Meteosat third generation - imaging 1 (MTG-I1)/FCI*

Meteosat Third Generation (MTG) is a collaborative program between EUMETSAT and ESA to promote operational European geostationary weather satellites. The program will comprise six satellites, including four imagery and two sounding satellites, providing improved weather forecasting, air quality monitoring, U.V. radiation alerts, and climate studies. MTG improves short-term and long-range forecasting by enabling near real-time storm tracking and providing detailed weather conditions. It also features lightning detection capabilities across Europe and Africa, benefiting numerical weather prediction models. MTG's mission ensures the continuity of geostationary data for climate studies and offers applications in firefighting, air traffic control, disaster management, agriculture, marine management, energy production, etc. The first satellite, MTG-I1 was launched in December 2022 and operates at a longitude 0°. It carries the instruments FCI (Flexible Combined Imager), LI (Lightning Imager), DCS (Data Collection System), and search and rescue from GEO (GEOSAR).

Meteosat Third Generation Imaging (MTG-I) satellites offer improved data frequency (full disk every 10 minutes), spatial resolution from 500 m to 2 km, and improved radiometric and spectral resolution, with 16 channels, compared to current MSG satellites. The Flexible Combined Imager (FCI) covers the visible spectrum (channels centred at 0.44, 0.51 and 0.64  $\mu\text{m}$ ), near-infrared (channels centred at 0.865, 0.914, 1.38, 1.61, and 2.25  $\mu\text{m}$ ) and infrared (channels centred at 3.80, 6.30, 7.35, 8.70, 9.66, 10.50, 12.30 and 13.30  $\mu\text{m}$ ),

surpassing its predecessor SEVIRI in radiometric, spectral and spatial capabilities. FCI's additional channels facilitate the detection of fine cirrus clouds, aerosols, and localized fire events, and operate in both standard and high spatial resolution modes, scanning Earth's disk every 10 minutes or selected regions every 2.5 minutes. The SNR from its visible and NIR bands varies from 12 to 40 with 1% albedo as input (European Space Agency 2022).

## 4. Recent applications of geostationary data over inland and coastal waters

### 4.1. Chlorophyll-a and algal organisms

One of the earliest studies on detecting algal blooms using geostationary data was conducted in 2012 using the world's first GOCI (Son, Min, and Ryu 2012). This study detected a massive bloom of floating green algae in the Yellow and East China Sea in 2011 and introduced the 'Index of floating Green Algae for GOCI' (IGAG) using multiple spectral band ratios based on the spectra of green algae. This method showed benefits in detecting subtle or less dense features when the water conditions were cloudy or complex. In the following years, several researchers reported the application of GOCI data to study photosynthetic organisms and their dynamics (Bao, Tian, and Chen 2015; Huang, Shi, et al. 2015; Qi et al. 2017). For example, GOCI data was used to determine chlorophyll-a (chl-a) concentrations using machine learning approaches (Y. H. Kim et al. 2014) and even to identify the physical factors affecting the distribution of floating green algae by combining GEO data and numerical methods, e. g. Lagrangian particle-tracking experiments (Son et al. 2015).

Identifying and monitoring algae in the most diverse water bodies is important issue due to its role in primary productivity and the imbalances caused to ecosystems. Chen et al. (2019) confirmed the ability of Himawari-8 in detecting and observing the distribution of floating algae in Lake Taihu, China. For this purpose, the Floating Algae Index (FAI) (Hu 2009) was adapted and compared to the results from the Moderate Resolution Imaging Spectroradiometer (MODIS) and GOCI, attesting the reliability Himawari-8/AHI estimates. Wang et al. (2022) developed a new method for automatic classification of cyanobacterial blooms and for the analysis of their diurnal changes. The method called 'diurnal change patterns classification' (DCPC) was proposed to Lake Taihu, a large eutrophic water body located in China. The work drew on a broad hourly dataset from the GOCI, classifying the observed patterns into four main types of daily changes of cyanobacteria blooms, including the decreasing (Type1), decreasing first and then increasing (Type2), increasing (Type3), increasing first and then decreasing (Type4).

In Yoon et al. (2019), chl-a estimation accuracy was assessed in a complex coastal region in Korea using GEO data and six algorithms. These included two standard open ocean algorithms, one GOCI-standard algorithm, and three regionally modified algorithms by Tassan for Korean waters (Tassan 1994). The study found that all tested algorithms tended to underestimate high chl-a concentrations highlighting the importance of adopting a regional approach to achieve accurate estimations in areas affected by anthropogenic activities. Recently, Yulong et al. (2022) introduced a novel approach called the BBHR (bio-optical – based hyperspectral reconstruction) method to estimate chl-a in complex inland waters. This method utilized six sensors coupled to various satellites, including GOCI, and employed a robust hyperspectral reconstruction technique

to generate remote sensing reflectance (Rrs). By training a multi-hyperspectral dictionary pair based on a bio-optical simulated Rrs dataset, the BBHR method became independent of *in situ* hyperspectral data, making it theoretically applicable universally. Additionally, two other recent studies focused on chl-a concentration estimation. One study adapted the three-band (TB) algorithm to GOCI data (Guo et al. 2022), while the other study detailed chl-a distribution using a new inversion model based on the relationship between *in situ* chl-a and spectral data from Gaofen-4, a Chinese GEO satellite (Bu et al. 2022).

Geostationary data have been utilized to directly explore the diurnal dynamics of cyanobacterial blooms in inland waters, employing spectral indices (Qi et al. 2018; S. Wang et al. 2022). Similarly, GEO data have been developed for monitoring harmful algal blooms in continental aquatic systems and coastal regions (Noh et al. 2018; Ye, Zhang, and Du 2022). The red tide phenomenon, characterized by rapid growth of protist phytoplankton causing harm to marine life, has garnered attention. Lee, Park, and Micheli (2021) investigated red tide using the Normalized Red Tide Index (NRTI), a specific spectral index based on GOCI sensor data and field data collected in the southern coastal region of the Korean peninsula. The NRTI relies on spectral characteristics across visible to near-infrared wavelengths. Table 1 summarizes essential details from papers that employed GEO data to investigate chlorophyll-a and algal organisms in inland and coastal waters, as presented in this review.

A pioneering study conducted by Lee et al. (2012) utilized GEO data from the GOCI instrument to investigate primary production in Taihu Lake, China. The study focused on assessing phytoplankton dynamics, diurnal variations in biomass, and available photosynthetic radiation. The integration of GOCI measurements significantly enhanced the accuracy of daily primary production estimates and provided valuable insights into the long-term dynamics of biogeochemical processes. Asaoka et al. (2020) adapted a model for estimating primary production and applied it to Hiroshima Bay, Japan. Notably, their approach capitalized on the use of data from a geostationary satellite, which offered superior spatial (~500 m) and temporal resolutions. This advancement enabled the estimation of coastal primary production even in areas with complex topography and smaller channels (<1 km). The utilization of geostationary satellite data represented a key differentiating factor of their study, showcasing its efficacy in improving our understanding of primary production dynamics in diverse coastal environments.

#### 4.2. Suspended solids and turbidity

In the early 2010s, GEO GOCI satellite data were utilized to study suspended materials in Asian lakes (Huang, Yang, et al. 2015; Lyu et al. 2015), estuaries (Cheng et al. 2016), and mostly in coastal regions of China and Korea (Choi et al. 2014; Eom et al. 2017; Y. H. Kim et al. 2014; K. Ruddick et al. 2012; Shen et al. 2014). An algorithm was developed to map the total suspended particulate matter (TSM) in Hangzhou Bay, the largest bay on China's southeastern coast (X. He et al. 2013). The study highlighted the diurnal dynamics in the bay and identified tides as the primary driver of spatial and temporal variations in TSM concentrations. Lyu et al. (2015) estimated the total suspended solid (TSS) concentration in different inland lakes in China by classifying simulated GOCI reflectance a bands from *in situ* measurements based in a clustering method. For each class, the authors developed

**Table 1.** Summary of GEO data-based research on chlorophyll-*a* and algal organisms in inland and coastal waters.

Autors, Year	GEO Satellite/ Sensor	Atmospheric correction – GEO data	Model or Index	Model accuracy* <sup>1</sup>	Observation period	Study area
Son et al. (2012)	COMS/ GOCI	'Second Simulation of a Satellite Signal in the Solar Spectrum' (6S) method Vermote et al. (1997).	'Index of floating Green Algae for GOCI' (IGAG). $IGAG = \frac{R(555) + R(660)}{R(745) - R(660)} + \frac{R(745)}{R(660)}$	-	Satellite images and <i>in situ</i> data collection: June and July, 2011.	Yellow Sea and East China Sea.
Bao, Tian and Chen (2015)	COMS/ GOCI	6S method Vermote et al. (1997).	Weighted Algorithm Based on Normalized Mutual Information.	MAE = 22.63% and RMSE = 9.41 mg/m <sup>3</sup> .	Satellite images: September 2011. <i>In situ</i> data collection: October and November 2010; March, September, and December 2011; and May 2012.	Taihu Lake.
Huang et al. (2015)	COMS/ GOCI	6S method Vermote et al. (1997).	Empirical C <sub>GHL-a</sub> (Chlorophyll- <i>a</i> concentration) NIR-red two-band algorithm. $C_{chl-a} = 10^{F(ratio)}$ $F(ratio) = 1.8875 + 0.8296 \cdot \left( 1 - 0.2241 \log \left( \frac{R(745)}{R(660)}, 10 \right) \right)$	R <sup>2</sup> = 0.71, N = 1126, <i>p</i> < 0.001, RMSP = 0.3644.	Satellite images: August 6 to August 9, 2013. <i>In situ</i> data collection: 2004 to 2013.	Taihu Lake.
Qi et al. (2017)	COMS/ GOCI	The data were corrected for Rayleigh scattering, but the method used was not specified in the paper.	'Alternative floating algae index' (AFAI). $AFAI = R_{rc\lambda_2} - R'_{rc\lambda_2}$ $R'_{rc\lambda_2} = R_{rc\lambda_1} + (R_{rc\lambda_3} - R_{rc\lambda_1})(\lambda_2 - \lambda_1)/(\lambda_3 - \lambda_1)$ where $\lambda_1$ , $\lambda_2$ , and $\lambda_3$ are 667, 748, and 869 nm for MODIS but adjusted for VIIRS, GOCI, and OLI using their corresponding bands. <i>R</i> <sub>rc</sub> correspond to Rayleigh-corrected reflectance	-	Satellite images: 2015 to 2017.	East China Sea

(Continued)

Table 1. (Continued).

Autors, Year	GEO Satellite/Sensor	Atmospheric correction – GEO data	Model or Index	Model accuracy*1	Observation period	Study area
Kim et al. (2014)	COMS/GOCI	Modified version of the original management unit of the north sea mathematical models (MUMM) algorithm by Ruddick, Ovidio, and Rijkeboer (2000).	Machine learning regression models: Random Forest (RF), Cubist, and Support Vector Regression (SVR).	Using <i>in situ</i> spectral samples: RF: $R^2 = 0.68$ , RMSE = $1.80 \text{ mg/m}^3$ (42.0%), CV (cross validation) RMSE = $1.80 \text{ mg/m}^3$ (42.1%). Cubist: $R^2 = 0.79$ , RMSE = $1.44 \text{ mg/m}^3$ (33.6%), CV RMSE = $1.92 \text{ mg/m}^3$ (44.9%). SVR: $R^2 = 0.86$ , RMSE = $1.18 \text{ mg/m}^3$ (27.5%), CV RMSE = $1.64 \text{ mg/m}^3$ (38.4%). Using GOCI-derived radiance data: RF: $R^2 = 0.57$ , RMSE = $2.09 \text{ mg/m}^3$ (48.8%), CV RMSE = $2.07 \text{ mg/m}^3$ (48.5%). Cubist: $R^2 = 0.79$ , RMSE = $1.48 \text{ mg/m}^3$ (34.7%), CV RMSE = $2.11 \text{ mg/m}^3$ (49.3%). SVR: $R^2 = 0.91$ , RMSE = $0.99 \text{ mg/m}^3$ (23.0%), CV RMSE = $1.74 \text{ mg/m}^3$ (40.7%).	Satellite images and <i>in situ</i> data collection: 11 June 2011, 26 October 2011, and 19–20 June 2012.	West coast of South Korea.
Son et al. (2015)	COMS/GOCI	GOCI Rayleigh-corrected reflectance with 6S method.	IGAG Son, Min, and Ryu (2012).	-	Satellite images: June and July 2011.	Yellow Sea and East China Sea.

(Continued)



Table 1. (Continued).

Autors, Year	GEO Satellite/Sensor	Atmospheric correction – GEO data	Model or Index	Model accuracy*1	Observation period	Study area
Chen et al. (2019)	Himawari-8/AHI	AHI Rayleigh-corrected reflectance following Hu et al. (2004) using 6S.	Floating Algae Index (FAI) developed by Hu (2009). $FAI = R_{TC,NIR} - R'_{TC,NIR}$ $R'_{TC,NIR} = R_{TC,RED} + (R_{TC,SWIR} - R_{TC,RED}) \cdot \frac{\lambda_{NIR} - \lambda_{RED}}{\lambda_{NIR} - \lambda_{RED}}$ where the subscripts refer to bands (RED = 640 nm, NIR = 860 nm, and SWIR = 1610 nm).	-	Satellite images: July 2015 to May 2018.	Taihu Lake.
Wang et al. (2022)	COMS/GOCI.	-	GOCI-derived alternative floating algae index (AFAI). $\beta_i = (AFAI_i - (-0.001)) / (0.12 - (-0.001))$	-	Satellite images: 2011 to 2020.	Taihu Lake.
Yoon et al. (2019)	COMS/GOCI	GOCI Data Processing System (GDPS, version 2.0).	where $\beta_i$ refers to the areal density of cyanobacterial blooms. Six ocean colour Chl-a algorithms: two standard open ocean algorithms (OC2S two-band ratio and OC3S three-band ratio NASA (2010), one GOCI-standard algorithm Moon et al. (2010), and three Tassan's algorithms regionally modified for Korean waters (Yellow Sea Large Marine Ecosystem Ocean Colour Project (YOC) algorithm Siswanto et al. (2011); Tassan (1994), Tassan-All and Tassan-TD algorithms W. Kim et al. (2016)).	OC2S: $r = 0.31$ ( $p > 0.05$ , $n = 22$ ), $S = 0.22$ , $I = -0.10$ , RMSE = 2.40, bias = -1.65. OC3S: $r = 0.32$ ( $p > 0.05$ , $n = 22$ ), $S = 0.26$ , $I = -0.16$ , RMSE = 2.46, bias = -1.75. GOCI-standard: $r = 0.45$ ( $p > 0.05$ , $n = 19$ ), $S = 2.51$ , $I = -0.47$ , RMSE = 3.34, bias = 0.59. YOC: $r = 0.51$ ( $p < 0.05$ , $n = 21$ ), $S = 1.39$ , $I = -0.19$ , RMSE = 2.52, bias = 0.03. Tassan-All: $r = 0.37$ ( $p > 0.05$ , $n = 22$ ), $S = 0.43$ , $I = -0.34$ , RMSE = 2.57, bias = -1.94. Tassan-TD: $r = 0.21$ ( $p > 0.05$ , $n = 22$ ), $S = 0.32$ , $I = -0.26$ , RMSE = 2.56, bias = -1.83.	Satellite images and in situ data collection: 2011 to 2016.	Jinhae Bay, southeastern coast of the Korean Peninsula.

(Continued)

Table 1. (Continued).

Authors, Year	GEO Satellite/ Sensor	Atmospheric correction – GEO data	Model or Index	Model accuracy*1	Observation period	Study area
Guo et al. (2022)	COMS/ GOCI	Improved land target-based atmospheric correction method Guanter et al. (2010); Liu et al. (2015).	Expanded Three Band (TB) Algorithm: MERIS TB $C_{chla} = 260.850 \times \frac{[R_s^{-1}(681) - R_s^{-1}(708)] R_s(753) + 26.342}{(R_s^2 = 0.878, P < 0.001)}$ GOCI TB $C_{chla} = 763.230 \times \frac{[R_s^{-1}(680) - R_s^{-1}(660)] R_s(745) - 4.485}{(R_s^2 = 0.823, P < 0.001)}$ GOCIBR (band ratio) $C_{chla} = 127.940 \times \frac{R_s(745)}{R_s(680)} - 35.436$ $(R^2 = 0.569, P < 0.001)$	The RMSE of the GOCI TB, MERIS TB, and GOCI BR algorithms are 14.212 µg/L, 12.096 µg/L, and 20.504 µg/L, respectively. The MAPE (when $C_{chla}$ is larger than 10 µg/L) of the three models were 0.377, 0.250, and 0.453, respectively.  $R^2 = 0.9123$ , RMSE = 0.1752 µg/L.	Satellite images and <i>in situ</i> data collection: 2013 to 2020.	The sampling areas covered several turbid waters in China, including Hongze Lake, Taihu Lake, Dongting Lake, Datong Lake, Changhu Lake, Honghu Lake, Huanggai Lake, Wushan Lake, Poyang Lake, Liangzi Lake, Huangda Lake, and Cihu Lake.
Bu et al. (2022)	GF-4/PMS	FLAAASH (Muchsin et al., 2019; Perkins, 2012).	Chl-a inversion model (named PMS-CJ): $p = 66.27x^2 - 14.751x + 3.3302$ $x = (R_s(\text{green}) - R_s(\text{red})) / (R_s(\text{blue}) + R_s(\text{green}))$		Satellite images: February 2020 to May 2021. <i>In situ</i> data collection: August 2020.	Yangtze River Mouth, eastern China.
Qi et al. (2018)	COMS/ GOCI	Rayleigh-corrected reflectance.	Alternative floating algae index (AFAI).	-	Satellite images: 2011 to 2016.	Taihu Lake.
Noh et al. (2018)	COMS/ GOCI	GOCI data processing (GDPS) software version 1.5 Ahn et al. (2015); Ahn et al. (2016).	The study developed a new red tide quantification algorithm. The proposed algorithm defines the red to blue ratio (RBR) as $RBR = \frac{R_{rs}(700)}{R_{rs}(490)}$  Sigmoidal type function between RBR and Chl-a: $log_{10} C = \frac{(p+qRBR^s)}{(1+RBR^s)}$ where $p = -0.19$ , $q = 2.51$ , $r = 0.21$ and $s = 1.02$ .	$R^2 = 0.92$ , RMSE = 107.87, MNGE = 63.5%, MNB = -44%.	Satellite images and <i>in situ</i> data collection: August 2013.	East Sea (Sea of Japan).
Lee et al. (2021)	COMS/ GOCI	Ahn et al. (2016).	New Normalized Red Tide Intensity Index (NRTI): Red Tide Intensity (RTI): $P555 = R_{rs}555 - \frac{660-555}{660-490} (R_{rs}490 - R_{rs}660)$ $P680 = R_{rs}680 - \frac{745-680}{745-660} (R_{rs}660 - R_{rs}745)$ $RTI = \frac{P555}{R_{rs}490} \times \frac{P680}{R_{rs}660}$ where P555 (P680) represents the first (second) peak height. $NRTI = \frac{RTI}{R_{rs}555 - R_{rs}745}$	RMSE = 2060, bias = -0.6913 cells mL <sup>-1</sup> , $R^2 = 0.7569$ , POD = 0.7068.	Satellite images and <i>in situ</i> data collection: 2012 to 2015.	Coastal region of Korean Peninsula.

\*1 Accuracy metrics: MAE = mean absolute error; RMSE = root mean square error;  $R^2$  = coefficient of determination; RMSP = root mean square error percentage;  $r$  = Pearson's correlation coefficient;  $S$  = slope;  $I$  = intercept; RMSE = root mean square deviation; MNGE = mean normalized gross error; MNB = mean normalized bias; POD = probability of detection.

a TSS concentration retrieval algorithm. According to the authors, this two-step approach exhibited significantly better performance compared to methods without pre-classification of water type.

In the past decade, the use of GEO satellites for estimating total suspended solids (TSS) has become more prevalent. For example, Dorji and Fearn (2018) assessed the applicability of the Himawari-8 satellite sensor for mapping TSS concentration in the coastal waters of Australia. The data underwent atmospheric correction using two different aerosol correction methods. The results indicated good performance in estimating concentrations above 0.15 mg/L at zenith angles below 60°. Additionally, strong correlations were observed in cross-validation with TSS concentration data derived from two other satellites, MODIS/Aqua and OLI/Landsat-8, with correlation coefficients ( $r^2$ ) of 0.71 and 0.91, respectively. Another study by Torres and Blanco (2021) utilized data from Himawari-8 to explore spatial approximations for chl-a and suspended solids, aiming to create high-frequency water quality maps for Manila Bay, Philippines.

Various approaches have been employed to study suspended solids in inland and coastal waters. Constantin et al. (2018) analysed river plumes using data from both geostationary and sun-synchronous polar orbit satellites. GEO satellite data revealed a strong connection between a French estuary's suspended particulate matter plume dynamics and the daily tidal cycle. Pan, Shen, and Wei (2018) fused data from GOCI and Landsat-8 to map suspended particulate matter with high temporal and spatial resolutions, achieving results with better accuracy when using the fused data. Shang and Xu (2018) developed a regional empirical modelling approach using geostationary data for suspended particle matter estimation, along with an algorithm for appropriate atmospheric correction. Liu et al. (2018) proposed an empirical algorithm based on a spectral absorption index to analyse diurnal and seasonal dynamics in coastal waters using GOCI data; the retrieved suspended matter values were consistent with *in situ* measurements. Table 2 provides a concise overview of key information extracted from publications that employed GEO data to investigate suspended solids in inland and coastal waters, as covered in this review.

Recently, Lin et al. (2022) retrieved time series information from a nine-year dataset of suspended sediment concentration obtained from hourly GOCI sensor images. Their findings, focusing on a coastal tidal basin in Jiangsu, China, revealed a strong influence of water level variations and wave intensity on the diurnal oscillation of suspended sediments. In the case of Lake Taihu in China, He et al. (2019) simulated the sedimentation process and monthly average sea surface temperature (SST) at the lake bottom using a numerical simulation combined with GOCI data. The GOCI data were atmospherically corrected using an algorithm based on ultraviolet wavelengths. The results provided valuable insights into critical areas prone to siltation.

GOCI sensor and *in situ* measurements were successfully applied to estimate the turbidity in estuaries in the coastal region of China. To tackle the complexity of these ecosystems, a machine learning technique, neural networks, was employed to develop a specific algorithm for turbidity estimation based on satellite-derived Rrs. Additionally, the study investigated the turbidity patterns associated with tidal action using numerical simulation and revealed an inverse relationship between turbidity and tidal height. Importantly, the algorithm demonstrated the potential to estimate turbidity values in areas beyond the training set (Feng et al. 2020).

Table 2. Summary of GEO data-based research on suspended solids in inland and coastal waters.

Autors, Year	GEO Satellite/ Sensor	Atmospheric correction – GEO data	Model type	Model accuracy*2	Observation period	Study area
Huang et al. (2015)	COMS/GOCI	6S method Vermote et al. (1997).	A combination of two (745 and 555 nm) and three-band (745, 680 and 555 nm) ratio algorithms was used. The depth of reflectance valley at 680 nm ( $R_{rs}$ -depth, 680) is considered as an index for deciding whether to utilize a two- ( $R_{rs}$ -depth, $680 \leq 0.005$ ) or three-band ( $R_{rs}$ -depth, $680 > 0.005$ ) algorithm in the combination algorithm.	RMSP = 34.52% for validation data and 45.01% for GOCI match-up points.	Satellite images and <i>in situ</i> data collection: May and August, 2013.	Taihu Lake.
Lyu et al., (2015)	COMS/GOCI	6S method Vermote et al. (1997).	Two-step retrieval method: first the <i>in situ</i> measured reflectance spectra were classified into several classes using a statistical clustering method, called the two-step clustering method SPSS (2001, 2004), then the appropriate retrieval algorithm was developed for estimating the TSS concentration for each class. The retrieval algorithms for the three classes of water:  $Class1$ $TSS = 412.3 \frac{Band6}{Band4} - 34.54$ $Class2$ $\ln TSS = 1.23 \ln \frac{Band7}{Band4}$ $Class3$ $\ln TSS = 1.46 \ln \frac{Band7}{Band4} + 2.24$	MAPE = 24.3% and RMSE = 16.5 mg l <sup>-1</sup> .	Satellite image: 13 May 2013. <i>In situ</i> data collection: 2008 to 2011.	Chinese inland lakes, i.e. Taihu Lake, Chaohu Lake, Dianchi Lake, and the Three Gorges Reservoir
Cheng et al. (2016)	COMS/GOCI	GDPS with the modified version of the MUMM algorithm J.-H. Ahn et al. (2012).	Regional algorithm by Yu (2013):  $lgC_{TSM} = 4.8581 + 0.8206 \frac{B7}{B3} - 0.9998 \frac{B4}{B3} - 3.6504 \sqrt{\frac{B3}{B3+B4}}$	RMSE = 9.11 g·m <sup>-3</sup> .	Satellite image: 2014. <i>In situ</i> data collection: August of 2009.	Yalu River, estuary of China.
Choi et al. (2014)	COMS/GOCI	MUMM (Management unit of the north sea Mathematical Models) algorithm developed by Ruddick, Ovidio, and Rijkeboer (2000).	where $C_{TSM}$ is surface TSM concentration in g·m <sup>-3</sup> and B represents the remote sensing reflectance (R <sub>rs</sub> ) corresponding to the central wavelengths of 4 bands (490 nm, 555 nm, 660 nm and 745 nm). Empirical TSM algorithm:  $TSM(\frac{a}{m}) = 1.545e^{179.53R_{rs}(660)}$	R <sup>2</sup> = 0.9269	Satellite images and <i>in situ</i> data collection: June 2011 and June 2012.	Gyeonggi Bay, Korea.

(Continued)

Table 2. (Continued).

Autors, Year	GEO Satellite/ Sensor	Atmospheric correction – GEO data	Model type	Model accuracy <sup>#2</sup>	Observation period	Study area
Eom et al. (2017)	COMS/GOCI	Modified MUMM algorithm	Empirical algorithm proposed by Choi et al. (2014).	-	Satellite images: 2012.	Gyeonggi Bay, Korea.
Kim et al., (2014)	COMS/GOCI	Modified MUMM algorithm.	Machine learning regression models: Random Forest (RF), Cubist, and Support Vector Regression (SVR).	Using <i>in situ</i> spectral samples: RF: R <sup>2</sup> = 0.90, RMSE = 11.92 g/m <sup>3</sup> (65.9%), CV RMSE = 12.19 g/m <sup>3</sup> (67.3%). Cubist: R <sup>2</sup> = 0.99, RMSE = 3.86 g/m <sup>3</sup> (21.3%), CV RMSE = 13.65 g/m <sup>3</sup> (75.4%). SVR: R <sup>2</sup> = 0.98, RMSE = 5.65 g/m <sup>3</sup> (31.2%). CV RMSE = 8.75 g/m <sup>3</sup> (48.3%). Using GOCI-derived radiance data: RF: R <sup>2</sup> = 0.87, RMSE = 13.47 g/m <sup>3</sup> (74.4%), CV RMSE = 14.21 g/m <sup>3</sup> (78.5%). Cubist: R <sup>2</sup> = 0.97, RMSE = 6.29 g/m <sup>3</sup> (34.7%). CV RMSE = 15.98 g/m <sup>3</sup> (88.3%). SVR: R <sup>2</sup> = 0.98, RMSE = 5.59 g/m <sup>3</sup> (30.9%), CV RMSE = 11.42 g/m <sup>3</sup> (63.1%).	Satellite image and <i>in situ</i> data collection: 11 June 2011, 26 October 2011, and 19–20 June 2012.	West coast of South Korea.

(Continued)

Table 2. (Continued).

Autors, Year	GEO Satellite/Sensor	Atmospheric correction – GEO data	Model type	Model accuracy*2	Observation period	Study area
Ruddick et al. (2012)	COMS/GOCI	GOCI Data Processing Software (GDPS), version 1.1.0 (dated 20120629). This atmospheric correction is based on the approach developed for SeaWiFS (Gordon and Wang 1994) but with an alternative treatment of the near infraredmarine reflectance in turbid waters.	GOCI standard TSS product, based on the algorithm of Y.-H. Ahn, Moon, and Gallegos (2001) and is a slightly non-linear function of Rrs555 given by Moon et al. (2010): $TSS = 945.07 \times (Rrs555)^{1.137}$	-	Satellite images: June and November, 2011.	Bohai Sea, China
Shen et al., (2014)	COMS/GOCI	Look-up-tables (LUTs), employing the atmospheric radiative transfer model (e.g. MODTRAN).	Recalibration of a semi-empirical radiative transfer model based on the Kubelka-Munk two-stream approximation of radiative transfer theory in water media Shen et al. (2010): $Rrs = \frac{a\beta C_{spm}}{1 + \beta C_{spm} + \sqrt{1 + 2\beta C_{spm}}}$ where Rrs refers to Remote-sensing reflectance (water-leaving reflectance), in units of inverse steradian, $\alpha$ and $\beta$ are the fitting constants, which can be recalibrated and optimized by <i>in situ</i> simultaneous measurements of remote-sensing reflectance, and the SPM concentration, $C_{spm}$ , in units of g/L, using the least squares method. Regional TSM algorithm for GOCI in the Hangzhou Bay: $\begin{cases} TSM = 10^{1.0758 + 1.1230 \times Ratio}, \\ (R = 0.96, SD = 0.22, N = 41, P < 0.0001) \\ Ratio = R_{rs}(745nm) / R_{rs}(490nm) \end{cases}$ where R and SD are the correlation coefficient and standard deviation, respectively.	-	<i>In situ</i> data collection: 2004 and 2012.	Yangtze estuary and adjacent coastal ocean, China.
He et al., (2013)	COMS/GOCI	Atmospheric correction algorithm for turbid waters using ultraviolet wavelengths (UV-AC) X. He and Pan (2003), adapted for GOCI bands.		The average relative bias and absolute relative errors are 13.3% and 25.2% for TSM $\leq$ 300 mg/l, and 14.2% and 56.0% for TSM >300 mg/l, respectively.	Satellite images: April and June, 2011. <i>In situ</i> data collection: July to August, 2006. December to February, 2007.	Hangzhou Bay, China.

(Continued)



Table 2. (Continued).

Autors, Year	Satellite/ Sensor	Atmospheric correction – GEO data	Model type	Model accuracy <sup>#2</sup>	Observation period	Study area
Dorji and Fearn (2018)	Himawari-8/ Advanced Himawari Imager (AHI)	It was presented an atmospheric correction method for AHI data using two different aerosol correction methods, a combination of two SWIR bands, and a combination of one NIR and one SWIR band.	Single red band TSS algorithm recalibrated from Dorji, Fearn, and Broomhall (2016): $AHI : TSS = \frac{22.12 \times (\frac{r}{\lambda})}{1 - 0.71 \times (\frac{r}{\lambda})} (R^2 = 0.89),$ where $x = \frac{-g + \sqrt{(g)^2 + 4g_2r_5(\lambda)}}{2g_2}$ , and $r_5(\lambda) = \frac{R_{rs}(\lambda)}{0.52 + 1.7R_{rs}(\lambda)} \cdot \lambda = (\text{band3}) (639.9 \text{ nm})$ for AHI, $g_1 = 0.084$ and $g_2 = 0.17$ . Regional algorithm for SEVIRI product: $SPM(gm^{-3}) = \frac{28.92R_{rs,625}}{(1 - R_{rs,625})/15.22}$	-	Satellites images and <i>in situ</i> data collection: July, 2015.	Pilbara coast, Western Australia.
Constantin et al. (2018)	Spinning Enhanced Visible and InfraRed Imager (SEVIRI)	Neukermans et al. (2009a).		$R^2 = 0.87$ , NRMSE = 10.9%.	GEO satellite images and <i>in situ</i> data collection: March 2014 and November 2016 to March 2017.	Gironde River plume, France.
Pan et al. (2018)	COMS/GOCI	Enhanced Spectral Optimization Algorithm (ESOA) (Pan, Shen, and Verhoef 2017) imbedded in the Level-2 generator (l2gen) program in the Sea-viewing Wide Field-of-View Sensor Data Analysis System (SeaDAS) software.	Semi-empirical model SERT Shen et al. (2010). $SPM = \frac{(\frac{\beta}{\alpha})R_{rs}}{(\alpha - R_{rs})^2}$ where $\alpha$ and $\beta$ are wavelength-dependent coefficients, which can be recalibrated and optimized by <i>in situ</i> simultaneous measurements of $R_{rs}$ and the [SPM]. Inversion scheme based on band shifting for SPM retrieval: $[SPM]^{GOCI} = \begin{cases} f_{inverse}(R_{rs,555}) \text{ if } R_{rs,660} < 0.012 \\ f_{inverse}(R_{rs,660}) \text{ else } R_{rs,865} < 0.02, \\ f_{inverse}(R_{rs,865}) \text{ else} \end{cases}$ Regional empirical model for GOCI: $\begin{cases} SPM = 10^{0.772 + 1.382X} \\ X = R_{rs,745} / R_{rs,490} \end{cases}$	Landsat-8/OLI and GOCI fused images: MRE = 17.7%. Only GOCI: MRE = 27.5%.	Satellite images and <i>in situ</i> data collection: August, September and November, 2013.	Yangtze (Changjiang) Estuary, China.
Shang and Xu (2018)	COMS/GOCI	GOCI level-2C Rayleigh corrected reflectance data acquired, follow by an aerosol scattering correction named UVAC algorithm (X. X. He et al. 2012).		$R^2 = 0.9376$ , RMSE = 89.32 mg/L	Satellite images: 2016. <i>In situ</i> data collection: March 2016, July 2016, August 2017 and July 2018.	Changjiang Estuary, China.

(Continued)

Table 2. (Continued).

Autors, Year	GEO Satellite/ Sensor	Atmospheric correction – GEO data	Model type	Model accuracy*2	Observation period	Study area
Liu et al. (2018)	COMS/GOCI	UVAC algorithm X. He, Pan, and Mao (2004).	New TSM algorithm based on SAI (spectral absorption index) D. Ma et al. (2016); J. Ma, Sun, and Pu (2016).  SAIindex : $SAI = \frac{dR_{0.490} + (1-d)R_{0.745}}{R_{0.555}}$ $d = \frac{555-490}{745-490}$ SAITSMalgorithm : $TSM = 10^{2.018145SAI+0.83774}$	R <sup>2</sup> = 0.8804, RPD = 24.48%, RMSE = 0.157.	Satellite images: 2013 to 2015. <i>In situ</i> data collection: April to May, 2013.	Hangzhou Bay, China.

\*2Accuracy metrics: RMSP = root mean square error percentage; MAPE = mean absolute percentage error; RMSE = Root Mean Square Error; R<sup>2</sup> = coefficient of determination; NRMSE = normalized root mean squared error; MRE = mean relative error; RPD = relative percentage difference.

## 5. Other applications

The phenomenon known as 'blue tide' and characterized by a blue colour on the water surface, results from the scattering of light by colloidal sulphur particles. The reaction of oxygen with resurgent hydrogen sulphide ( $H_2S$ ) produced by anaerobic bacteria in deep waters causes this phenomenon. Blue tides can lead to the mass mortality of aquatic organisms, including fish and crustaceans. Using data obtained by the GOCI satellite, researchers were able to observe and analyse the distribution of blue tides in a bay in the centre of Japan. Sulphur concentration data were used to develop an empirical model that estimates sulphur concentration based on the logarithm of  $R_{rs}$  at a wavelength of  $0.660\ \mu m$ . This study conducted by Higa et al. (2020) provides valuable insights into understanding and monitoring the occurrence of blue tides in coastal waters.

Water transparency, typically measured by Secchi disk depth (SDD), serves as a fundamental water quality indicator. Based on GOCI data, Bai et al. (2020) improved the accuracy of estimating water transparency in eutrophic waters by linearly fitting a well-established model developed by Lee et al. (2015). They incorporated field data to correct the model, demonstrating the reliability of estimating SDD using remote sensing reflectance. Similarly, Zhou et al. (2022) proposed a linearly corrected regional model for SDD estimation in Jiaozhou Bay, utilizing GOCI data and SDD estimation models from North Sea Mathematical Models and Lee et al. (2015). Their multivariate linear regression analysis highlighted the influence of solar zenith angle (SZA) and tides on diurnal SDD variations in the bay.

The presence of particulate organic carbon (POC) in water bodies such as rivers and estuaries has garnered significant interest. Liu et al. (2019) utilized hourly data from the COMS (GOCI) satellite to develop algorithms for estimating the monthly flow of POC in the Changjiang River estuary, China. This estimation was based on the observed nearly-linear relationship between POC and TSM, derived from *in situ* measurements. Subsequently, Wang et al. (2021) conducted a follow-up POC flow study in the same area. They combined POC concentration data estimated from GOCI images with a numerical model to assess its flux and distribution, aiming to support long-term monitoring in estuaries and gain insights into the effects of terrestrial inputs in marginal seas.

In addition to these studies, GEO satellites sensors have been applied in various other areas. Goldberg et al. (2018) employed them for flood monitoring, Huang, Hu, and Shi (2021) focused on coastal upwelling mapping, Du et al. (2021) utilized them for water quality assessment, and Bracaglia et al. (2020) used them to create new virtual geostationary datasets. These diverse applications demonstrate the versatility of GEO satellites sensors in different aspects of water monitoring and research.

## 6. Summary and future work

Over the past decade, the use of geostationary data in inland and coastal waters has demonstrated its potential to provide reliable information, enhancing our understanding of daily and hourly water dynamics. Although the number of publications in this field is limited compared to studies focused on the oceans and atmosphere, the application of geostationary datasets has proven effective in gaining insights into recent research. Notably, the majority of these studies have been conducted in

Asia, indicating the unexplored potential of utilizing geostationary data in other parts of the world. These findings highlight the promising opportunities for further investigation and usage of geostationary data in various regions and scientific domains.

The use of geostationary satellites sensors, such as GOCI and AHI, has significantly advanced our understanding on various aspects of inland and coastal waters. These sensors provided information on the dynamics of chlorophyll-a concentration, algal blooms, suspended solids, turbidity, and other water quality indicators. Generating corrected products, like the ones provided by GEONEX simplifying data interpretation and improving the usability of geostationary data for a wide range of applications. Furthermore, the potential for the fusion of geostationary data with other satellite systems, such as MODIS, offers an excellent opportunity to improve temporal revisit rates and increase the capacity of predictive models.

However, there are still obstacles to overcome in order to fully utilize the potential of geostationary satellites sensors in inland and coastal water applications. Not all algorithms have been rigorously validated with geostationary data, requiring greater refinement and validation efforts. The generally lower spatial resolution and challenges in atmospheric correction and managing large volumes of data are other issues that require attention. Questions such as the balance between high temporal resolution and the spatial detail provided by geostationary satellites sensors, the effectiveness of these sensors in overcoming cloud cover problems in images, and possible comparative differences between the results of sun-synchronous satellites sensors and geostationary satellites sensors are still to be explored. Such challenges could provide a starting point for future research, promising even deeper insights and solutions in developing monitoring and understanding of the planet's invaluable water resources.

## Disclosure statement

No potential conflict of interest was reported by the author(s).

## Funding

This work was supported by the Coordenação de Aperfeiçoamento de Pessoal de Nível Superior—Brasil (CAPES) - Finance Code 001.

## ORCID

Carina F. Portela  <http://orcid.org/0000-0002-5627-3783>

Cláudio C. F. Barbosa  <http://orcid.org/0000-0002-3221-9774>

## References

- Ahn, Y.-H., J.-E. Moon, and S. Gallegos. 2001. "Development of Suspended Particulate Matter Algorithms for Ocean Color Remote Sensing." *Korean Journal of Remote Sensing* 17 (4): 285–295.
- Ahn, J., Park, Y., Kim, W, and Lee, B. 2016. "Simple aerosol correction technique based on the spectral relationships of the aerosol multiple-scattering reflectances for atmospheric correction over the oceans." *Optics Express*, 24 (26): 29659. <https://doi.org/10.1364/OE.24.029659>.

- Ahn, J., Park, Y., Kim, W., Lee, B., and Oh, I.-S. 2015. "Vicarious calibration of the Geostationary Ocean Color Imager." *Optics Express*, 23(18): 23236. <https://doi.org/10.1364/OE.23.023236>.
- Ahn, J.-H., Y.-J. Park, J.-H. Ryu, B. Lee, and I. S. Oh. 2012. "Development of Atmospheric Correction Algorithm for Geostationary Ocean Color Imager (GOCI)." *Ocean Science Journal* 47 (3): 247–259. <https://doi.org/10.1007/s12601-012-0026-2>.
- Allard, M. 2006. 'Noaa's NowCOAST: A Gis-Web Mapping Portal to Discover and Display Real-Time Coastal Observations, Satellite Imagery and NOAA Forecasts'. In *15th Symposium on Education*, Atlanta, Georgia, United States of America.
- Apel, J. R. 1980. "Satellite Sensing of Ocean Surface Dynamics." *Annual Review of Earth and Planetary Sciences* 8 (1): 303–342. <https://doi.org/10.1146/annurev.ea.08.050180.001511>.
- Aranha, T. R. B. T., J.-M. Martinez, E. P. Souza, M. U. G. Barros, and E. S. P. R. Martins. 2022. "Remote Analysis of the Chlorophyll-A Concentration Using Sentinel-2 MSI Images in a Semiarid Environment in Northeastern Brazil." *Water* 14 (3): 451. <https://doi.org/10.3390/w14030451>.
- Asaoka, S., S. Nakada, A. Umehara, J. Ishizaka, and W. Nishijima. 2020. "Estimation of Spatial Distribution of Coastal Ocean Primary Production in Hiroshima Bay, Japan, with a Geostationary Ocean Color Satellite." *Estuarine, Coastal and Shelf Science* 244:106897. <https://doi.org/10.1016/j.ecss.2020.106897>.
- Bai, S., J. Gao, D. Sun, and M. Tian. 2020. "Monitoring Water Transparency in Shallow and Eutrophic Lake Waters Based on GOCI Observations." *Remote Sensing* 12 (1): 163.
- Bao, Y., Q. Tian, and M. Chen. 2015. "A Weighted Algorithm Based on Normalized Mutual Information for Estimating the Chlorophyll-A Concentration in Inland Waters Using Geostationary Ocean Color Imager (GOCI) Data." *Remote Sensing* 7 (9): 11731–11752. <https://doi.org/10.3390/rs70911731>.
- Barrett, E. C., and M. G. Hamilton. 1982. "The Use of Geostationary Satellite Data in Environmental Science." *Progress in Physical Geography: Earth and Environment* 6 (2): 159–214. <https://doi.org/10.1177/030913338200600201>.
- Barton, I., and A. Pearce. 2006. "Validation of GLI and Other Satellite-Derived Sea Surface Temperatures Using Data from the Rottnest Island Ferry, Western Australia." *Journal of Oceanography* 62 (3): 303–310. <https://doi.org/10.1007/s10872-006-0055-5>.
- Bernardo, N., E. Alcântara, F. Watanabe, T. Rodrigues, A. Carmo, A. Gomes, and C. Andrade. 2018. "Glint Removal Assessment to Estimate the Remote Sensing Reflectance in Inland Waters with Widely Differing Optical Properties." *Remote Sensing* 10 (10): 1655. <https://doi.org/10.3390/rs10101655>.
- Bessho, K., K. Date, M. Hayashi, A. Ikeda, T. Imai, H. Inoue, Y. Kumagai, T. Miyakawa, H. Murata, and T. Ohno. 2016. "An Introduction to Himawari-8/9—Japan's New-Generation Geostationary Meteorological Satellites." *Journal of the Meteorological Society of Japan* 94 (2): 151–183. <https://doi.org/10.2151/jmsj.2016-009>.
- Bracaglia, M., R. Santoleri, G. Volpe, S. Colella, M. Benincasa, and V. Ernesto Brando. 2020. "A Virtual Geostationary Ocean Color Sensor to Analyze the Coastal Optical Variability." *Remote Sensing* 12 (10): 1539. <https://doi.org/10.3390/rs12101539>.
- Brezonik, P., K. D. Menken, and M. Bauer. 2005. "Landsat-Based Remote Sensing of Lake Water Quality Characteristics, Including Chlorophyll and Colored Dissolved Organic Matter (CDOM)." *Lake and Reservoir Management* 21 (4): 373–382. <https://doi.org/10.1080/074381140509354442>.
- Bu, J., L. Cai, X. Yan, H. Xu, H. Hu, and J. Jiang. 2022. "Monitoring the Chl-A Distribution Details in the Yangtze River Mouth Using Satellite Remote Sensing." *Water* 14 (8): 1295. <https://doi.org/10.3390/w14081295>.
- Bulgarelli, B., and G. Zibordi. 2018. "On the Detectability of Adjacency Effects in Ocean Color Remote Sensing of Mid-Latitude Coastal Environments by SeaWiFS, MODIS-A, MERIS, OLCI, OLI and MSI." *Remote Sensing of Environment* 209:423–438. [10.1016/j.rse.2017.12.021](https://doi.org/10.1016/j.rse.2017.12.021).
- Capderou, M. 2014. *Handbook of Satellite Orbits: From Kepler to GPS*. Cham, Switzerland: Springer Science & Business.
- Castelao, R. M., T. P. Mavor, J. A. Barth, and L. C. Breaker. 2006. "Sea Surface Temperature Fronts in the California Current System from Geostationary Satellite Observations." *Journal of Geophysical Research Oceans* 111 (C9). <https://doi.org/10.1029/2006JC003541>.

- Chamberlin, J. L. 1982. "Application of Satellite Infrared Data to Analysis of Ocean Frontal Movements and Water Mass Interactions off Northeastern United States." *Stud* 4:21–30.
- Cheng, Z., X. Hua Wang, D. Paull, and J. Gao. 2016. "Application of the Geostationary Ocean Color Imager to Mapping the Diurnal and Seasonal Variability of Surface Suspended Matter in a Macro-Tidal Estuary." *Remote Sensing* 8 (3): 244. <https://doi.org/10.3390/rs8030244>.
- Chen, S., L. Han, X. Chen, D. Li, L. Sun, and Y. Li. 2015. "Estimating Wide Range Total Suspended Solids Concentrations from MODIS 250-M Imageries: An Improved Method." *Isprs Journal of Photogrammetry & Remote Sensing* 99:58–69. [10.1016/j.isprsjprs.2014.10.006](https://doi.org/10.1016/j.isprsjprs.2014.10.006).
- Chen, X., S. Shang, Z. Lee, L. Qi, J. Yan, and Y. Li. 2019. "High-Frequency Observation of Floating Algae from AHI on Himawari-8." *Remote Sensing of Environment* 227:151–161. <https://doi.org/10.1016/j.rse.2019.03.038>.
- Chen, J., Y. Wu, S. Wu, L. Xie, J. Tang, Z. Xu, X. Han, et al. 2023. "Application of FY-4B Geostationary Meteorological Satellite in Grassland Fire Dynamic Monitoring." *IEEE Transactions on Geoscience and Remote Sensing* 61:1–9. <https://doi.org/10.1109/TGRS.2023.3274630>.
- Choi, J.-K., Y. Je Park, J. Hyun Ahn, H.-S. Lim, J. Eom, and J.-H. Ryu. 2012. "GOCI, the World's First Geostationary Ocean Color Observation Satellite, for the Monitoring of Temporal Variability in Coastal Water Turbidity." *Journal of Geophysical Research Oceans* 117 (C9). <https://doi.org/10.1029/2012JC008046>.
- Choi, J.-K., Y. Je Park, B. R. Lee, J. Eom, J.-E. Moon, and J.-H. Ryu. 2014. "Application of the Geostationary Ocean Color Imager (GOCI) to Mapping the Temporal Dynamics of Coastal Water Turbidity." *Remote Sensing of Environment* 146:24–35. [10.1016/j.rse.2013.05.032](https://doi.org/10.1016/j.rse.2013.05.032).
- Choi, J.-K., M.-S. Park, K.-S. Han, H.-C. Kim, and J. Im. 2021. "One Year of GOCI-II Launch Present and Future." *대한원격탐사학회*. <https://doi.org/10.7780/kjrs.2021.37.5.2.1>.
- Clarke, A. C. 1945. "Extra-Terrestrial Relays." *Electronics World* 119 (1924): 14–19.
- Constantin, S., D. Doxaran, A. Derkacheva, S. Novoa, and H. Lavigne. 2018. "Multi-Temporal Dynamics of Suspended Particulate Matter in a Macro-Tidal River Plume (The Gironde) as Observed by Satellite Data." *Estuarine, Coastal and Shelf Science* 202:172–184. <https://doi.org/10.1016/j.ecss.2018.01.004>.
- Darnell, W. L., and R. C. Harriss. 1983. "Satellite Sensing Capabilities for Surface Temperature and Meteorological Parameters Over the Ocean." *International Journal of Remote Sensing* 4 (1): 65–92. <https://doi.org/10.1080/01431168308948531>.
- Davis, C. O., and M. Abbott. 2005. 'A New Capability for Monitoring the Coastal Ocean from Geostationary Orbit'. In *Proceedings of OCEANS 2005 MTS/IEEE*, 1459–1463. Washington, D.C., United States of America: IEEE.
- Dorji, P., and P. Fearn. 2018. "Atmospheric Correction of Geostationary Himawari-8 Satellite Data for Total Suspended Sediment Mapping: A Case Study in the Coastal Waters of Western Australia." *Isprs Journal of Photogrammetry & Remote Sensing* 144:81–93. <https://doi.org/10.1016/j.isprsjprs.2018.06.019>.
- Dorji, P., P. Fearn, and M. Broomhall. 2016. "A Semi-Analytic Model for Estimating Total Suspended Sediment Concentration in Turbid Coastal Waters of Northern Western Australia Using MODIS-Aqua 250 M Data." *Remote Sensing* 8 (7): 556.
- Duan, H., R. Ma, Y. Zhang, S. Arthur Loiselle, J. Xu, C. Zhao, L. Zhou, and L. Shang. 2010. "A New Three-Band Algorithm for Estimating Chlorophyll Concentrations in Turbid Inland Lakes." *Environmental Research Letters* 5 (4): 044009. <https://doi.org/10.1088/1748-9326/5/4/044009>.
- Du, Z., J. Qi, S. Wu, F. Zhang, and R. Liu. 2021. "A Spatially Weighted Neural Network Based Water Quality Assessment Method for Large-Scale Coastal Areas." *Environmental Science & Technology* 55 (4): 2553–2563. [10.1021/acs.est.0c05928](https://doi.org/10.1021/acs.est.0c05928).
- Emberton, S., L. Chittka, A. Cavallaro, and M. Wang. 2016. "Sensor Capability and Atmospheric Correction in Ocean Colour Remote Sensing." *Remote Sensing* 8 (1): 1. <https://doi.org/10.3390/rs8010001>.
- Eom, J., J.-K. Choi, J.-S. Won, J.-H. Ryu, D. Doxaran, K. Ruddick, and S. Lee. 2017. "Spatiotemporal Variation in Suspended Sediment Concentrations and Related Factors of Coastal Waters Based on Multispatial Satellite Data in Gyeonggi Bay, Korea." *Journal of Financial Stability* 33 (3): 653–667. <https://doi.org/10.2112/JCOASTRES-D-16-00012.1>.



- European Space Agency. 2022. 'Satellite Missions Catalogue'. <https://www.eoportal.org/satellite-missions>.
- Feng, J., H. Chen, H. Zhang, Z. Li, Y. Yu, Y. Zhang, M. Bilal, and Z. Qiu. 2020. "Turbidity Estimation from GOCI Satellite Data in the Turbid Estuaries of China's Coast." *Remote Sensing* 12 (22): 3770. <https://doi.org/10.3390/rs12223770>.
- Fu, S., X. Lou, J. Yang, P. Wang, W. Guan, and D. Fu. 2021. 'Multi-Satellite Observation of a Harmful Algal Bloom in the Beibu Gulf, South China Sea'. In *2021 Photonics & Electromagnetics Research Symposium (PIERS)*, 2329–2335. Hangzhou, Zhejiang, China: IEEE.
- Garriott, O. K., F. L. Smith, and P. C. Yuen. 1965. "Observations of Ionospheric Electron Content Using a Geostationary Satellite." *Planetary & Space Science* 13 (8): 829–838. [https://doi.org/10.1016/0032-0633\(65\)90119-4](https://doi.org/10.1016/0032-0633(65)90119-4).
- Ghilain, N., A. Arboleda, O. Batelaan, J. Ardö, I. Trigo, J.-M. Barrios, and F. Gellens-Meulenberghs. 2019. "A New Retrieval Algorithm for Soil Moisture Index from Thermal Infrared Sensor On-Board Geostationary Satellites Over Europe and Africa and Its Validation." *Remote Sensing* 11 (17): 1968. <https://doi.org/10.3390/rs11171968>.
- Gholizadeh, M. H., A. M. Melesse, and L. Reddi. 2016. "A Comprehensive Review on Water Quality Parameters Estimation Using Remote Sensing Techniques." *Sensors* 16 (8): 1298. <https://doi.org/10.3390/s16081298>.
- Giardino, C., M. Pepe, P. Alessandro Brivio, P. Ghezzi, and E. Zilioli. 2001. "Detecting Chlorophyll, Secchi Disk Depth and Surface Temperature in a Sub-Alpine Lake Using Landsat Imagery." *Science of the Total Environment* 268 (1): 19–29. [https://doi.org/10.1016/S0048-9697\(00\)00692-6](https://doi.org/10.1016/S0048-9697(00)00692-6).
- Goldberg, M. D., S. Li, S. Goodman, D. Lindsey, B. Sjöberg, and D. Sun. 2018. "Contributions of Operational Satellites in Monitoring the Catastrophic Floodwaters Due to Hurricane Harvey." *Remote Sensing* 10 (8): 1256. <https://doi.org/10.3390/rs10081256>.
- Gordon, H. R., and M. Wang. 1994. "Retrieval of Water-Leaving Radiance and Aerosol Optical Thickness Over the Oceans with SeaWiFS: A Preliminary Algorithm." *Applied Optics* 33 (3): 443–452. <https://doi.org/10.1364/AO.33.000443>.
- Groom, S., S. Sathyendranath, Y. Ban, S. Bernard, R. Brewin, V. Brotas, C. Brockmann, et al. 2019. "Satellite Ocean Colour: Current Status and Future Perspective." *Frontiers in Marine Science* 6. <https://doi.org/10.3389/fmars.2019.00485>.
- Guan, Q., L. Feng, X. Hou, G. Schurgers, Y. Zheng, and J. Tang. 2020. "Eutrophication Changes in Fifty Large Lakes on the Yangtze Plain of China Derived from MERIS and OLCI Observations." *Remote Sensing of Environment* 246:111890. <https://doi.org/10.1016/j.rse.2020.111890>.
- Guanter, L., Ruiz-Verdú, A., Odermatt, D., Giardino, C., Simis, S., Estellés, V., Heege, T., Domínguez-Gómez, J. Antonio, and Moreno, J. 2010. "Atmospheric correction of ENVISAT/MERIS data over inland waters: Validation for European lakes." *Remote Sensing of Environment* 114 3: 467–480. <https://doi.org/10.1016/j.rse.2009.10.004>.
- Günthner, K., I. Khan, D. Elser, B. Stiller, Ö. Bayraktar, C. R. Müller, K. Saucke, et al. 2017. "Quantum-Limited Measurements of Optical Signals from a Geostationary Satellite." *Optica* 4 (6): 611–616. <https://doi.org/10.1364/OPTICA.4.000611>.
- Guo, Y., C. Huang, Y. Li, C. Du, Y. Li, W. Chen, L. Shi, and G. Ji. 2022. "An Expanded Three Band Model to Monitor Inland Optically Complex Water Using Geostationary Ocean Color Imager (GOCI)." *Frontiers in Remote Sensing* 3:3. <https://doi.org/10.3389/frsen.2022.803884>.
- Hadjimitsis, D. G., and C. Clayton. 2009. "Assessment of Temporal Variations of Water Quality in Inland Water Bodies Using Atmospheric Corrected Satellite Remotely Sensed Image Data." *Environmental Monitoring and Assessment* 159 (1): 281–292. <https://doi.org/10.1007/s10661-008-0629-3>.
- He, X., Y. Bai, D. Pan, N. Huang, X. Dong, J. Chen, and Q. Cui. 2013. "Using Geostationary Satellite Ocean Color Data to Map the Diurnal Dynamics of Suspended Particulate Matter in Coastal Waters." *Remote Sensing of Environment* 133:225–239. <https://doi.org/10.1016/j.rse.2013.01.023>.
- He, X., Y. Bai, D. Pan, J. Tang, and D. Wang. 2012. "Atmospheric Correction of Satellite Ocean Color Imagery Using the Ultraviolet Wavelength for Highly Turbid Waters." *Optics Express* 20 (18): 20754–20770. <https://doi.org/10.1364/OE.20.020754>.

- He, A., X. He, Y. Bai, Q. Zhu, F. Gong, H. Huang, and D. Pan. 2019. "Simulation of Sedimentation in Lake Taihu with Geostationary Satellite Ocean Color Data." *Remote Sensing* 11 (4): 379. <https://doi.org/10.3390/rs11040379>.
- He, X., and D. Pan. 2003. "Practical Method of Atmospheric Correction of SeaWiFS Imagery for Turbid Coastal and Inland Waters." . In *Proceedings of the Conference on Ocean Remote Sensing and Applications*. 24–26 October 2003. Hangzhou, China.
- He, X., D. Pan, and Z. Mao. 2004. "Atmospheric Correction of SeaWiFS Imagery for Turbid Coastal and Inland Waters." *Acta Oceanologica Sinica* 23 (4): 609–615.
- Heta, Y., and Y. Mitsuta. 1993. "An Evaluation of Evaporation Over the Tropical Pacific Ocean as Observed from Satellites." *Journal of Applied Meteorology* 32 (7): 1242–1247. [https://doi.org/10.1175/1520-0450\(1993\)032<1242:AEOTEOT>2.0.CO;2](https://doi.org/10.1175/1520-0450(1993)032<1242:AEOTEOT>2.0.CO;2).
- Higa, H., S. Sugahara, S. Ibrahim Salem, Y. Nakamura, and T. Suzuki. 2020. "An Estimation Method for Blue Tide Distribution in Tokyo Bay Based on Sulfur Concentrations Using Geostationary Ocean Color Imager (GOCI)." *Estuarine, Coastal and Shelf Science* 235:106615. <https://doi.org/10.1016/j.ecss.2020.106615>.
- Higuchi, A. 2021. "Toward More Integrated Utilizations of Geostationary Satellite Data for Disaster Management and Risk Mitigation." *Remote Sensing* 13 (8): 1553. <https://doi.org/10.3390/rs13081553>.
- Højerslev, N. K. 1980. "Water Color and Its Relation to Primary Production." *Boundary-Layer Meteorology* 18 (2): 203–220. <https://doi.org/10.1007/BF00121324>.
- Holtorf, C., and A. Piccini. 2009. *Contemporary Archaeologies: Excavating Now*. Frankfurt: Peter Lang.
- Hu, C. 2009. "A Novel Ocean Color Index to Detect Floating Algae in the Global Oceans." *Remote Sensing of Environment* 113 (10): 2118–2129. <https://doi.org/10.1016/j.rse.2009.05.012>.
- Huang, Z., and M. Feng. 2021. "MJO Induced Diurnal Sea Surface Temperature Variations off the Northwest Shelf of Australia Observed from Himawari Geostationary Satellite." *Deep Sea Research Part II: Topical Studies in Oceanography* 183:104925. <https://doi.org/10.1016/j.dsr2.2021.104925>.
- Huang, Z., J. Hu, and W. Shi. 2021. "Mapping the Coastal Upwelling East of Taiwan Using Geostationary Satellite Data." *Remote Sensing* 13 (2): 170. <https://doi.org/10.3390/rs13020170>.
- Huang, C., K. Shi, H. Yang, Y. Li, A. X. Zhu, D. Sun, L. Xu, J. Zou, and X. Chen. 2015. "Satellite Observation of Hourly Dynamic Characteristics of Algae with Geostationary Ocean Color Imager (GOCI) Data in Lake Taihu." *Remote Sensing of Environment* 159:278–287. <https://doi.org/10.1016/j.rse.2014.12.016>.
- Huang, C., H. Yang, A. X. Zhu, M. Zhang, H. Lü, T. Huang, J. Zou, and Y. Li. 2015. "Evaluation of the Geostationary Ocean Color Imager (GOCI) to Monitor the Dynamic Characteristics of Suspension Sediment in Taihu Lake." *International Journal of Remote Sensing* 36 (15): 3859–3874. <https://doi.org/10.1080/01431161.2015.1070323>.
- Hubert, L. F., and L. F. Whitney. 1971. "Wind Estimation from Geostationary-Satellite Pictures." *Monthly Weather Review* 99 (9): 665–672. [https://doi.org/10.1175/1520-0493\(1971\)099<0665:WEGP>2.3.CO;2](https://doi.org/10.1175/1520-0493(1971)099<0665:WEGP>2.3.CO;2).
- Hu, C., Chen, Z., Clayton, T D., Swarzenski, P., Brock, J.-C, and Muller-Karger, F.-E. 2004. "Assessment of estuarine water-quality indicators using MODIS medium-resolution bands: Initial results from Tampa Bay, FL." *Remote Sensing of Environment* 93 (3): 423–441. <https://doi.org/10.1016/j.rse.2004.08.007>.
- Ilori, C. O., N. Pahlevan, and A. Knudby. 2019. "Analyzing Performances of Different Atmospheric Correction Techniques for Landsat 8: Application for Coastal Remote Sensing." *Remote Sensing* 11 (4): 469. <https://doi.org/10.3390/rs11040469>.
- IOCCG2006 Remote Sensing of Inherent Optical Properties: Fundamentals, Tests of Algorithms, and Applications edited by N. Z.-P. Lee Vol. 5 Reports of the International Ocean Colour Coordinating Group Dartmouth, Canada IOCCG <https://doi.org/10.25607/OBP-96>
- IOCCG2012 Ocean-Colour Observations from a Geostationary Orbited edited by N. D. Antoine Vol. 12 Reports of the International Ocean Colour Coordinating Group Dartmouth, Canada IOCCG <https://doi.org/10.25607/OBP-103>

- IOCCG2018 Earth Observations in Support of Global Water Quality Monitoring edited by N. S. Greb, A. Dekker, and C. Binding. Vol. 17. *Reports of the International Ocean Colour Coordinating Group*. Dartmouth, Canada: IOCCG. <https://doi.org/10.25607/OBP-113>
- Jiang, H., N. Lu, J. Qin, W. Tang, and L. Yao. 2019. "A Deep Learning Algorithm to Estimate Hourly Global Solar Radiation from Geostationary Satellite Data." *Renewable and Sustainable Energy Reviews* 114:109327. <https://doi.org/10.1016/j.rser.2019.109327>.
- Jo, Y.-H., X.-H. Yan, and F. Li. 2010. "Potential Applications of Geostationary Ocean Color Imagery for Physical-Biological Interactions." In *Geostationary Ocean Color Imager (GOCI) Technical Development, Operation, and Applications*, edited by Y.-H. Ahn, D. Antoine, P. S. Bontempi, and D. Pan, Vol. 7861, 78610C. SPIE. <https://doi.org/10.1117/12.869097>.
- Kay, S., J. D. Hedley, and S. Lavender. 2009. "Sun Glint Correction of High and Low Spatial Resolution Images of Aquatic Scenes: A Review of Methods for Visible and Near-Infrared Wavelengths." *Remote Sensing* 1 (4): 697–730. <https://doi.org/10.3390/rs1040697>.
- Kazi, L. I. 1990. *Infrared and Visible Studies of Pakistan Portion of Arabian Sea Using INSAT Geostationary Satellite*. University of Miami.
- Kim, Y. H., J. Im, H. K. Ha, J.-K. Choi, and S. Ha. 2014. "Machine Learning Approaches to Coastal Water Quality Monitoring Using GOCI Satellite Data." *GIScience & Remote Sensing* 51 (2): 158–174. <https://doi.org/10.1080/15481603.2014.900983>.
- Kim, W., J.-E. Moon, Y.-J. Park, and J. Ishizaka. 2016. "Evaluation of Chlorophyll Retrievals from Geostationary Ocean Color Imager (GOCI) for the North-East Asian Region." *Remote Sensing of Environment* 184:482–495. <https://doi.org/10.1016/j.rse.2016.07.031>.
- Kirk, J. T. 2010. *Light and Photosynthesis in Aquatic Ecosystems*. Third Edit. Cambridge, UK: Cambridge University Press.
- Koffler, R. 1975. 'Use of NOAA Environmental Satellites to Remotely Sense Ocean Phenomena'. In *OCEAN 75 Conference*, 835–839. <https://doi.org/10.1109/OCEANS.1975.1154116>.
- Kutser, T., E. Vahtmäe, and J. Praks. 2009. "A Sun Glint Correction Method for Hyperspectral Imagery Containing Areas with Non-Negligible Water Leaving NIR Signal." *Remote Sensing of Environment* 113 (10): 2267–2274. <https://doi.org/10.1016/j.rse.2009.06.016>.
- Lee, B., J. H. Ahn, Y.-J. Park, and S.-W. Kim. 2013. "Turbid Water Atmospheric Correction for GOCI: Modification of MUMM Algorithm." *Korean Journal of Remote Sensing* 29 (2): 173–182. <https://doi.org/10.7780/kjrs.2013.29.2.2>.
- Lee, Z., M. Jiang, C. Davis, N. Pahlevan, Y.-H. Ahn, and R. Ma. 2012. "Impact of Multiple Satellite Ocean Color Samplings in a Day on Assessing Phytoplankton Dynamics." *Ocean Science Journal* 47 (3): 323–329. <https://doi.org/10.1007/s12601-012-0031-5>.
- Lee, Y., C. Jung, and S. Kim. 2019. "Spatial Distribution of Soil Moisture Estimates Using a Multiple Linear Regression Model and Korean Geostationary Satellite (COMS) Data." *Agricultural Water Management* 213:580–593. <https://doi.org/10.1016/j.agwat.2018.09.004>.
- Lee, M.-S., K.-A. Park, and F. Micheli. 2021. "Derivation of Red Tide Index and Density Using Geostationary Ocean Color Imager (GOCI) Data." *Remote Sensing* 13 (2): 298. <https://doi.org/10.3390/rs13020298>.
- Lee, Z., S. Shang, C. Chuanmin, K. Du, A. Weidemann, W. Hou, J. Lin, and G. Lin. 2015. "Secchi Disk Depth: A New Theory and Mechanistic Model for Underwater Visibility." *Remote Sensing of Environment* 169:139–149. <https://doi.org/10.1016/j.rse.2015.08.002>.
- Legeckis, R. 1978. "A Survey of Worldwide Sea Surface Temperature Fronts Detected by Environmental Satellites." *Journal of Geophysical Research Oceans* 83 (C9): 4501–4522. <https://doi.org/10.1029/JC083iC09p04501>.
- Legeckis, R., C. W. Brown, and P. S. Chang. 2002. "Geostationary Satellites Reveal Motions of Ocean Surface Fronts." *Journal of Marine Systems* 37 (1–3): 3–15. [https://doi.org/10.1016/S0924-7963\(02\)00192-6](https://doi.org/10.1016/S0924-7963(02)00192-6).
- Legeckis, R., W. Pichel, and G. Nesterczuk. 1983. "Equatorial Long Waves in Geostationary Satellite Observations and in a Multichannel Sea Surface Temperature Analysis." *Bulletin of the American Meteorological Society* 64 (2): 133–139. [https://doi.org/10.1175/1520-0477\(1983\)064<0133:ELWIGS>2.0.CO;2](https://doi.org/10.1175/1520-0477(1983)064<0133:ELWIGS>2.0.CO;2).

- Legeckis, R., and T. Zhu. 1997. "Sea Surface Temperatures from the GOES-8 Geostationary Satellite." *Bulletin of the American Meteorological Society* 78 (9): 1971–1984. [https://doi.org/10.1175/1520-0477\(1997\)078<1971:SSTFTG>2.0.CO;2](https://doi.org/10.1175/1520-0477(1997)078<1971:SSTFTG>2.0.CO;2).
- Letelier, R. M., and M. R. Abbott. 1996. "An Analysis of Chlorophyll Fluorescence Algorithms for the Moderate Resolution Imaging Spectrometer (MODIS)." *Remote Sensing of Environment* 58 (2): 215–223. [https://doi.org/10.1016/S0034-4257\(96\)00073-9](https://doi.org/10.1016/S0034-4257(96)00073-9).
- Li, H. 2014. *Geostationary Satellites Collocation*. Berlin: Springer.
- Liang, S., J. Wang, and B. Jiang. 2012. A Systematic View of Remote Sensing. *Advanced Remote Sensing*. (pp. 1–31). Oxford: Academic Press.
- Lima, T. M. A., C. Giardino, M. Bresciani, C. C. F. Barbosa, A. Fabbretto, A. Pellegrino, and F. Nincao Begliomini. 2023. "Assessment of Estimated Phycocyanin and Chlorophyll-A Concentration from PRISMA and OLCI in Brazilian Inland Waters: A Comparison Between Semi-Analytical and Machine Learning Algorithms." *Remote Sensing* 15 (5): 1299. <https://doi.org/10.3390/rs15051299>.
- Lin, H., Q. Yu, Y. Wang, and S. Gao. 2022. "Identification, Extraction and Interpretation of Multi-Period Variations of Coastal Suspended Sediment Concentration Based on Unevenly Spaced Observations." *Marine Geology* 445:106732. <https://doi.org/10.1016/j.margeo.2022.106732>.
- Liu, D., Y. Bai, X. He, B. Tao, D. Pan, C.-T. A. Chen, L. Zhang, Y. Xu, and C. Gong. 2019. "Satellite Estimation of Particulate Organic Carbon Flux from Changjiang River to the Estuary." *Remote Sensing of Environment* 223:307–319. <https://doi.org/10.1016/j.rse.2019.01.025>.
- Liu, G., Li, Y., Lyu, H., Wang, S., Du, C, and Huang, C. 2015. "An Improved Land Target-Based Atmospheric Correction Method for Lake Taihu." *IEEE J. Sel. Top. Appl. Earth Observations Remote Sensing*, 9(2), 793–803. [10.1109/JSTARS.2015.2503800](https://doi.org/10.1109/JSTARS.2015.2503800)
- Liu, J., J. Liu, X. He, D. Pan, Y. Bai, F. Zhu, T. Chen, and Y. Wang. 2018. "Diurnal Dynamics and Seasonal Variations of Total Suspended Particulate Matter in Highly Turbid Hangzhou Bay Waters Based on the Geostationary Ocean Color Imager." *IEEE Journal of Selected Topics in Applied Earth Observations & Remote Sensing* 11 (7): 2170–2180. <https://doi.org/10.1109/JSTARS.2018.2830335>.
- Li, F., X. Zhang, D. P. Roy, and S. Kondragunta. 2019. "Estimation of Biomass-Burning Emissions by Fusing the Fire Radiative Power Retrievals from Polar-Orbiting and Geostationary Satellites Across the Conterminous United States." *Atmospheric Environment* 211:274–287. <https://doi.org/10.1016/j.atmosenv.2019.05.017>.
- Lomax, A. S., D. W. Colburn, and M. K. Galbraith. 2006. "The Value of Geostationary Satellite Imagery in IOOS, Now and Future." *Oceans* 1–5. <https://doi.org/10.1109/OCEANS.2006.306822>.
- Lyu, H., J. Zhang, G. Zha, Q. Wang, and Y. Li. 2015. "Developing a Two-Step Retrieval Method for Estimating Total Suspended Solid Concentration in Chinese Turbid Inland Lakes Using Geostationary Ocean Colour Imager (GOCI) Imagery." *International Journal of Remote Sensing* 36 (5): 1385–1405. <https://doi.org/10.1080/01431161.2015.1009654>.
- Ma, D., J. Liu, J. Y. Huang, H. Li, P. Liu, H. Chen, and J. Qian. 2016. "Spectral Similarity Assessment Based on a Spectrum Reflectance-Absorption Index and Simplified Curve Patterns for Hyperspectral Remote Sensing." *Sensors* 16 (2): 152. <https://doi.org/10.3390/s16020152>.
- Martins, V. S., C. Clemente Faria Barbosa, L. Augusto Sander De Carvalho, D. Schaffer Ferreira Jorge, and F. De Lucia Lobo. 2017. "Assessment of Atmospheric Correction Methods for Sentinel-2 MSI Images Applied to Amazon Floodplain Lakes." *Remote Sensing* 9 (4): 322. <https://doi.org/10.3390/rs9040322>.
- Martins, V. S., A. Kaleita, C. C. F. Barbosa, A. C. Fassoni-Andrade, F. de Lucia Lobo, and E. M. L. M. Novo. 2019. "Remote Sensing of Large Reservoir in the Drought Years: Implications on Surface Water Change and Turbidity Variability of Sobradinho Reservoir (Northeast Brazil)." *Remote Sensing Applications: Society & Environment* 13:275–288. <https://doi.org/10.1016/j.rsase.2018.11.006>.
- Ma, J., D.-W. Sun, and H. Pu. 2016. "Spectral Absorption Index in Hyperspectral Image Analysis for Predicting Moisture Contents in Pork Longissimus Dorsi Muscles." *Food Chemistry* 197:848–854. <https://doi.org/10.1016/j.foodchem.2015.11.023>.
- Maturi, E., A. Harris, C. Merchant, J. Mittaz, B. Potash, W. Meng, and J. Sapper. 2008. "Noaa's Sea Surface Temperature Products from Operational Geostationary Satellites." *Bulletin of the American Meteorological Society* 89 (12): 1877–1888. <https://doi.org/10.1175/2008BAMS2528.1>.

- Maul, G. A., P. Webb DeWitt, A. Yanaway, and S. R. Baig. 1978. "Geostationary Satellite Observations of Gulf Stream Meanders: Infrared Measurements and Time Series Analysis." *Journal of Geophysical Research Oceans* 83 (C12): 6123–6135. <https://doi.org/10.1029/JC083iC12p06123>.
- McClain, E. P. 1980. "Passive Radiometry of the Ocean from Space—An Overview." *Boundary-Layer Meteorology* 18 (1): 7–24. <https://doi.org/10.1007/BF00117908>.
- McCorkel, J., B. Efremova, J. Hair, M. Andrade, and B. Holben. 2020. "GOES-16 ABI Solar Reflective Channel Validation for Earth Science Application." *Remote Sensing of Environment* 237:111438. <https://doi.org/10.1016/j.rse.2019.111438>.
- Merchant, C. J., P. Le Borgne, H. Roquet, and A. Marsouin. 2009. "Sea Surface Temperature from a Geostationary Satellite by Optimal Estimation." *Remote Sensing of Environment* 113 (2): 445–457. <https://doi.org/10.1016/j.rse.2008.10.012>.
- Miller, S. D., C. C. Schmidt, T. J. Schmit, and D. W. Hillger. 2012. "A Case for Natural Colour Imagery from Geostationary Satellites, and an Approximation for the GOES-R ABI." *International Journal of Remote Sensing* 33 (13): 3999–4028. <https://doi.org/10.1080/01431161.2011.637529>.
- Minghelli, A., C. Chevalier, J. Descloitres, L. Berline, P. Blanc, and M. Chami. 2021. "Synergy Between Low Earth Orbit (LEO)—MODIS and Geostationary Earth Orbit (GEO)—GOES Sensors for Sargassum Monitoring in the Atlantic Ocean." *Remote Sensing* 13 (8): 1444. <https://doi.org/10.3390/rs13081444>.
- Mobley, C. D. 1999. "Estimation of the Remote-Sensing Reflectance from Above-Surface Measurements." *Applied Optics* 38 (36): 7442–7455. <https://doi.org/10.1364/AO.38.007442>.
- Moon, J.-E., Y.-H. Ahn, J.-H. Ryu, and P. Shanmugam. 2010. "Development of Ocean Environmental Algorithms for Geostationary Ocean Color Imager (GOCI)." *Korean Journal of Remote Sensing* 26 (2): 189–207.
- Moses, W. J., S. Sterckx, M. J. Montes, L. De Keukelaere, and E. Knaeps. 2017. "Chapter 3 - Atmospheric Correction for Inland Waters." In *Bio-Optical Modeling and Remote Sensing of Inland Waters*, edited by D. R. Mishra, I. Ogashawara, and A. A. Gitelson, 69–100. Elsevier. <https://doi.org/10.1016/B978-0-12-804644-9.00003-3>.
- Mota, B., and M. J. Wooster. 2018. "A New Top-Down Approach for Directly Estimating Biomass Burning Emissions and Fuel Consumption Rates and Totals from Geostationary Satellite Fire Radiative Power (FRP)." *Remote Sensing of Environment* 206:45–62. <https://doi.org/10.1016/j.rse.2017.12.016>.
- Muchsin, F., Dirghayu, D., Prasasti, I., Rahayu, M.-I., Fibriawati, L., Pradono, K.-A., and Mahatmanto, B. 2019. "Comparison of atmospheric correction models: FLAASH and 6S code and their impact on vegetation indices (case study: paddy field in Subang District, West Java)." *IOP Conference Series: Earth and Environmental Science*, 280 (1): 012034. <https://doi.org/10.1088/1755-1315/280/1/012034>.
- Murakami, H. 2016. "Ocean Color Estimation by Himawari-8/AHI." In *Remote Sensing of the Oceans and Inland Waters: Techniques, Applications, and Challenges*, edited by R. J. Frouin, S. C. Shenoi, and K. H. Rao, Vol. 9878, 987810. SPIE. <https://doi.org/10.1117/12.2225422>.
- NASA. 2010. "Ocean Color Chlorophyll (OC) V6". <https://oceancolor.gsfc.nasa.gov/reprocessing/r2009/ocv6/>.
- Neukermans, G., K. Ruddick, E. Bernard, D. Ramon, B. Nechad, and P.-Y. Deschamps. 2009a. "Mapping Total Suspended Matter from Geostationary Satellites: A Feasibility Study with SEVIRI in the Southern North Sea." *Optics Express* 17 (16): 14029–14052. <https://doi.org/10.1364/OE.17.014029>.
- Neukermans, G., K. Ruddick, E. Bernard, D. Ramon, B. Nechad, and P.-Y. Deschamps. 2009b. "Mapping Total Suspended Matter from Geostationary Satellites: A Feasibility Study with SEVIRI in the Southern North Sea." *Optics Express* 17 (16): 14029–14052. <https://doi.org/10.1364/OE.17.014029>.
- Neukermans, G., K. G. Ruddick, and N. Greenwood. 2012. "Diurnal Variability of Turbidity and Light Attenuation in the Southern North Sea from the SEVIRI Geostationary Sensor." *Remote Sensing of Environment* 124:564–580. <https://doi.org/10.1016/j.rse.2012.06.003>.



- Noh, J. H., W. Kim, S. Hyun Son, J.-H. Ahn, and Y.-J. Park. 2018. "Remote Quantification of *Cochlodinium Polykrikoides* Blooms Occurring in the East Sea Using Geostationary Ocean Color Imager (GOCI)." *Harmful Algae* 73:129–137. <https://doi.org/10.1016/j.hal.2018.02.006>.
- Novoa, S., D. Doxaran, A. Ody, Q. Vanhellemont, V. Lafon, B. Lubac, and P. Gernez. 2017. "Atmospheric Corrections and Multi-Conditional Algorithm for Multi-Sensor Remote Sensing of Suspended Particulate Matter in Low-To-High Turbidity Levels Coastal Waters." *Remote Sensing* 9 (1): MDPI: 61.
- Ogashawara, I., D. R. Mishra, and A. G. Anatoly. 2017. "Chapter 1 - Remote Sensing of Inland Waters: Background and Current State-Of-The-Art". In *Bio-Optical Modeling and Remote Sensing of Inland Waters*, In edited by D. R. Mishra, I. Ogashawara, and A. A. Gitelson, 1–24. Elsevier. [10.1016/B978-0-12-804644-9.00001-X](https://doi.org/10.1016/B978-0-12-804644-9.00001-X).
- Overstreet, B. T., and C. J. Legleiter. 2017. "Removing Sun Glint from Optical Remote Sensing Images of Shallow Rivers." *Earth Surface Processes and Landforms* 42 (2): 318–333. <https://doi.org/10.1002/esp.4063>.
- Paek, S. W., S. Kim, L. Kronig, and O. De Weck. 2020. "Sun-Synchronous Repeat Ground Tracks and Other Useful Orbits for Future Space Missions." *Aeronautical Journal* 124 (1276): 917–939. <https://doi.org/10.1017/aer.2020.21>.
- Pahlevan, N., B. Smith, J. Schalles, C. Binding, Z. Cao, R. Ma, K. Alikas, et al. 2020. "Seamless Retrievals of Chlorophyll-A from Sentinel-2 (MSI) and Sentinel-3 (OLCI) in Inland and Coastal Waters: A Machine-Learning Approach." *Remote Sensing of Environment* 240:111604. <https://doi.org/10.1016/j.rse.2019.111604>.
- Pan, Y., S. Bélanger, and Y. Huot. 2022. "Evaluation of Atmospheric Correction Algorithms Over Lakes for High-Resolution Multispectral Imagery: Implications of Adjacency Effect." *Remote Sensing* 14 (13): 2979. <https://doi.org/10.3390/rs14132979>.
- Pan, Y., F. Shen, and W. Verhoef. 2017. "An Improved Spectral Optimization Algorithm for Atmospheric Correction Over Turbid Coastal Waters: A Case Study from the Changjiang (Yangtze) Estuary and the Adjacent Coast." *Remote Sensing of Environment* 191:197–214. <https://doi.org/10.1016/j.rse.2017.01.013>.
- Pan, Y., F. Shen, and X. Wei. 2018. "Fusion of Landsat-8/OLI and GOCI Data for Hourly Mapping of Suspended Particulate Matter at High Spatial Resolution: A Case Study in the Yangtze (Changjiang) Estuary." *Remote Sensing* 10 (2): 158. <https://doi.org/10.3390/rs10020158>.
- Park, K.-A., H.-J. Woo, and E.-Y. Lee. 2020. "The Application of a Hybrid Sea Surface Temperature Algorithm to COMS Geostationary Satellite Data in the Northwest Pacific Ocean." *International Journal of Remote Sensing* 41 (15): 5953–5973. <https://doi.org/10.1080/01431161.2019.1688889>.
- Paulino, R. S., V. S. Martins, E. M. L. M. Novo, C. C. F. Barbosa, L. A. S. de Carvalho, and F. N. Begliomini. 2022. "Assessment of Adjacency Correction Over Inland Waters Using Sentinel-2 MSI Images." *Remote Sensing* 14 (8): 1829. <https://doi.org/10.3390/rs14081829>.
- Pereira, G., K. M. Longo, S. R. Freitas, G. Mataveli, V. J. Oliveira, P. R. Santos, L. F. Rodrigues, and F. S. Cardozo. 2022. "Improving the South America Wildfires Smoke Estimates: Integration of Polar-Orbiting and Geostationary Satellite Fire Products in the Brazilian Biomass Burning Emission Model (3BEM)." *Atmospheric Environment* 273:118954. <https://doi.org/10.1016/j.atmosenv.2022.118954>.
- Perkins T. 2012. "Speed and accuracy improvements in FLAASH atmospheric correction of hyperspectral imagery." *Optical Engineering*, 51 (11): 111707. <https://doi.org/10.1117/1.OE.51.11.111707>.
- Pozdnyakov, D., H. Grassl, and H. Graßl. 2003. *Color of Inland and Coastal Waters: A Methodology for Its Interpretation*. Berlin: Springer Science & Business Media.
- Preisendorfer, R. W. 1976. *Hydrologic Optics*. Honolulu: US Department of Commerce, National Oceanic and Atmospheric Administration.
- Qi, L., C. Hu, P. M. Visser, and R. Ma. 2018. "Diurnal Changes of Cyanobacteria Blooms in Taihu Lake as Derived from GOCI Observations." *Limnology & Oceanography* 63 (4): 1711–1726. <https://doi.org/10.1002/lno.10802>.
- Qi, L., C. Hu, M. Wang, S. Shang, and C. Wilson. 2017. "Floating Algae Blooms in the East China Sea." *Geophysical Research Letters* 44 (22): ,11,501–11,509. <https://doi.org/10.1002/2017GL075525>.



- Rajan, D., A. K. Bohra, A. K. Mitra, V. S. Prasad, R. K. Paliwal, and V. B. Bhatia. 2002. "Moisture Profiles from Satellite Data Over the Indian Ocean Area." *International Journal of Remote Sensing* 23 (15): 2951–2969. <https://doi.org/10.1080/01431160110075316>.
- Ritchie, J. C., C. M. Cooper, and F. R. Schiebe. 1990. "The Relationship of MSS and TM Digital Data with Suspended Sediments, Chlorophyll, and Temperature in Moon Lake, Mississippi." *Remote Sensing of Environment* 33 (2): 137–148. [https://doi.org/10.1016/0034-4257\(90\)90039-O](https://doi.org/10.1016/0034-4257(90)90039-O).
- Ruddick, K., G. Neukermans, Q. Vanhellemont, and D. Jolivet. 2014. "Challenges and Opportunities for Geostationary Ocean Colour Remote Sensing of Regional Seas: A Review of Recent Results." *Remote Sensing of Environment* 146:63–76. <https://doi.org/10.1016/j.rse.2013.07.039>.
- Ruddick, K. G., F. Ovidio, and M. Rijkeboer. 2000. "Atmospheric Correction of SeaWiFS Imagery for Turbid Coastal and Inland Waters." *Applied Optics* 39 (6): 897–912. <https://doi.org/10.1364/AO.39.000897>.
- Ruddick, K., Q. Vanhellemont, J. Yan, G. Neukermans, G. Wei, and S. Shang. 2012. "Variability of Suspended Particulate Matter in the Bohai Sea from the Geostationary Ocean Color Imager (GOCI)." *Ocean Science Journal* 47 (3): 331–345. <https://doi.org/10.1007/s12601-012-0032-4>.
- Ryu, J. H., J. K. Choi, J. Eom, and J. H. Ahn. 2011. "Temporal Variation in Korean Coastal Waters Using Geostationary Ocean Color Imager." *Journal of Coastal Research* 64 1731–1735.
- Sagan, V., K. T. Peterson, M. Maimaitijiang, P. Sidike, J. Sloan, B. A. Greeling, S. Maalouf, and C. Adams. 2020. "Monitoring Inland Water Quality Using Remote Sensing: Potential and Limitations of Spectral Indices, Bio-Optical Simulations, Machine Learning, and Cloud Computing." *Earth Science Review* 205:103187. <https://doi.org/10.1016/j.earscirev.2020.103187>.
- Santer, R., and C. Schmechtig. 2000. "Adjacency Effects on Water Surfaces: Primary Scattering Approximation and Sensitivity Study." *Applied Optics* 39 (3): 361–375. <https://doi.org/10.1364/AO.39.000361>.
- Schmit, T. J., P. Griffith, M. M. Gunshor, J. M. Daniels, S. J. Goodman, and W. J. Lehair. 2017. "A Closer Look at the ABI on the GOES-R Series." *Bulletin of the American Meteorological Society* 98 (4): 681–698. <https://doi.org/10.1175/BAMS-D-15-00230.1>.
- Schmit, T. J., S. S. Lindstrom, J. J. Gerth, and M. M. Gunshor. 2018. "Applications of the 16 Spectral Bands on the Advanced Baseline Imager (ABI)." *Journal of Operational Meteorology* 6 (04): 33–46. <https://doi.org/10.15191/nwajom.2018.0604>.
- Shang, D., and H. Xu. 2018. "Qualitative Dynamics of Suspended Particulate Matter in the Changjiang Estuary from Geostationary Ocean Color Images: An Empirical, Regional Modeling Approach." *Sensors* 18 (12): MDPI: 4186. <https://doi.org/10.3390/s18124186>.
- Shen, F., W. Verhoef, Y. Zhou, M. Suhyb Salama, and X. Liu. 2010. "Satellite Estimates of Wide-Range Suspended Sediment Concentrations in Changjiang (Yangtze) Estuary Using MERIS Data." *Estuaries & Coasts* 33 (6): 1420–1429. <https://doi.org/10.1007/s12237-010-9313-2>.
- Shen, F., Y. Zhou, X. Peng, and Y. Chen. 2014. "Satellite Multi-Sensor Mapping of Suspended Particulate Matter in Turbid Estuarine and Coastal Ocean, China." *International Journal of Remote Sensing* 35 (11–12): 4173–4192. <https://doi.org/10.1080/01431161.2014.916053>.
- Shu, L., L. Zhu, J. Bak, P. Zoogman, H. Han, X. Long, B. Bai, S. Liu, D. Wang, and W. Sun. 2022. "Improved Ozone Simulation in East Asia via Assimilating Observations from the First Geostationary Air-Quality Monitoring Satellite: Insights from an Observing System Simulation Experiment." *Atmospheric Environment* 274:119003. <https://doi.org/10.1016/j.atmosenv.2022.119003>.
- Siswanto, E., J. Tang, H. Yamaguchi, Y.-H. Ahn, J. Ishizaka, S. Yoo, S.-W. Kim, Y. Kiyomoto, K. Yamada, and C. Chiang. 2011. "Empirical Ocean-Color Algorithms to Retrieve Chlorophyll-A, Total Suspended Matter, and Colored Dissolved Organic Matter Absorption Coefficient in the Yellow and East China Seas." *Journal of Oceanography* 67 (5): 627–650. <https://doi.org/10.1007/s10872-011-0062-z>.
- Son, Y. B., B.-J. Choi, Y. Hoon Kim, and Y.-G. Park. 2015. "Tracing Floating Green Algae Blooms in the Yellow Sea and the East China Sea Using GOCI Satellite Data and Lagrangian Transport Simulations." *Remote Sensing of Environment* 156:21–33. <https://doi.org/10.1016/j.rse.2014.09.024>.

- Song, Z., X. He, Y. Bai, X. Dong, D. Wang, T. Li, Q. Zhu, and F. Gong. 2023. "Atmospheric Correction of Absorbing Aerosols for Satellite Ocean Color Remote Sensing Over Coastal Waters." *Remote Sensing of Environment* 290:113552. <https://doi.org/10.1016/j.rse.2023.113552>.
- Son, Y. B., J.-E. Min, and J.-H. Ryu. 2012. "Detecting Massive Green Algae (*Ulva Prolifera*) Blooms in the Yellow Sea and East China Sea Using Geostationary Ocean Color Imager (GOCI) Data." *Ocean Science Journal* 47 (3): 359–375. <https://doi.org/10.1007/s12601-012-0034-2>.
- Soop, E. M. 1994. *Handbook of Geostationary Orbits*. New York, USA: Springer Science & Business Media.
- Sowden, M., U. Mueller, and D. Blake. 2018. "Review of Surface Particulate Monitoring of Dust Events Using Geostationary Satellite Remote Sensing." *Atmospheric Environment* 183:154–164. <https://doi.org/10.1016/j.atmosenv.2018.04.020>.
- SPSS. 2001. *The SPSS TwoStep Cluster Component: A Scalable Component Enabling More Efficient Customer Segmentation. Technical Report*. SPSS Chicago, IL.
- SPSS. 2004. 'Two Step Cluster Analysis'. *Technical Report*. SPSS Chicago, IL.
- Tarpley, J. D. 1979. "Estimating Incident Solar Radiation at the Surface from Geostationary Satellite Data." *Journal of Applied Meteorology and Climatology* 18 (9): 1172–1181. [https://doi.org/10.1175/1520-0450\(1979\)018<1172:EISRAT>2.0.CO;2](https://doi.org/10.1175/1520-0450(1979)018<1172:EISRAT>2.0.CO;2).
- Tassan, S. 1994. "Local Algorithms Using SeaWiFS Data for the Retrieval of Phytoplankton, Pigments, Suspended Sediment, and Yellow Substance in Coastal Waters." *Applied Optics* 33 (12): 2369–2378. <https://doi.org/10.1364/AO.33.002369>.
- Torres, R. B., and A. C. Blanco. 2021. "Preliminary Investigation on Chlorophyll-A and Total Suspended Matter Concentration in Manila Bay Using HIMAWARI-8 Ahi and SENTINEL-3 Olci C2RCC." *International Archives of the Photogrammetry, Remote Sensing and Spatial Information Sciences* 46:303–311. <https://doi.org/10.5194/isprs-archives-XLVI-4-W6-2021-303-2021>.
- Union of Concerned Scientists. 2022. 'UCS Satellite Database'. <https://www.ucsusa.org/resources/satellite-database>.
- Uudeberg, K., A. Aavaste, K.-L. Kõks, A. Ansper, M. Uusõue, K. Kangro, I. Ansko, M. Ligi, K. Toming, and A. Reinart. 2020. "Optical Water Type Guided Approach to Estimate Optical Water Quality Parameters." *Remote Sensing* 12 (6): 931. <https://doi.org/10.3390/rs12060931>.
- Vermote, E. F., D. Tanré, J. L. Deuze, M. Herman, and J.-J. Morcrette. 1997. "Second Simulation of the Satellite Signal in the Solar Spectrum, 6S: An Overview." *IEEE Transactions on Geoscience & Remote Sensing* 35 (3): 675–686. <https://doi.org/10.1109/36.581987>.
- Wang, Z., Y. Bai, X. He, B. Tao, T. Li, X. Chen, T. Wang, and F. Gong. 2021. "Estimating Particulate Organic Carbon Flux in a Highly Dynamic Estuary Using Satellite Data and Numerical Modeling." *Remote Sensing of Environment* 252:112116. <https://doi.org/10.1016/j.rse.2020.112116>.
- Wang, S., Y. Mao, L. Zheng, Z. Qiu, M. Bilal, and D. Sun. 2020. "Remote Sensing of Water Turbidity in the Eastern China Seas from Geostationary Ocean Colour Imager." *International Journal of Remote Sensing* 41 (11): 4080–4101. <https://doi.org/10.1080/01431161.2020.1714775>.
- Wang, M., W. Shi, and L. Jiang. 2012. "Atmospheric Correction Using Near-Infrared Bands for Satellite Ocean Color Data Processing in the Turbid Western Pacific Region." *Optics Express* 20 (2): 741–753. <https://doi.org/10.1364/OE.20.000741>.
- Wang, S., X. Zhang, N. Chen, and W. Wang. 2022. "Classifying Diurnal Changes of Cyanobacterial Blooms in Lake Taihu to Identify Hot Patterns, Seasons and Hotspots Based on Hourly GOCI Observations." *Journal of Environmental Management* 310:114782. <https://doi.org/10.1016/j.jenvman.2022.114782>.
- Watanabe, T., H. Takenaka, and D. Nohara. 2021. "Post-Processing Correction Method for Surface Solar Irradiance Forecast Data from the Numerical Weather Model Using Geostationary Satellite Observation Data." *Solar Energy* 223:202–216. <https://doi.org/10.1016/j.solener.2021.05.055>.
- World Meteorological Organization. 2022. 'Observing Systems Capability Analysis and Review Tool (OSCAR)'. <https://space.oscar.wmo.int/>.
- Wu, Y., A. Knudby, and D. Lapen. 2023. "Topography-Adjusted Monte Carlo Simulation of the Adjacency Effect in Remote Sensing of Coastal and Inland Waters." *Journal of Quantitative Spectroscopy & Radiative Transfer* 303:108589. <https://doi.org/10.1016/j.jqsrt.2023.108589>.

- Yang, J., Z. Zhang, C. Wei, F. Lu, and Q. Guo. 2017. "Introducing the New Generation of Chinese Geostationary Weather Satellites, Fengyun-4." *Bulletin of the American Meteorological Society* 98 (8): 1637–1658. [10.1175/BAMS-D-16-0065.1](https://doi.org/10.1175/BAMS-D-16-0065.1).
- Yan, Q.-Y., P. Leng, Z.-L. Li, Q.-Y. Liao, F.-C. Zhou, X.-J. Han, J. Ma, Y.-Y. Sun, X. Zhang, and G.-F. Shang. 2022. "A Method for Estimating Spatially Continuous Soil Moisture from the Synergistic Use of Geostationary and Polar-Orbit Satellite Data." *Journal of Hydrology* 608:127590.
- Yeom, J.-M., R. C. Deo, J. F. Adamowski, S. Park, and C.-S. Lee. 2020. "Spatial Mapping of Short-Term Solar Radiation Prediction Incorporating Geostationary Satellite Images Coupled with Deep Convolutional LSTM Networks for South Korea." *Environmental Research Letters* 15 (9): 094025. <https://doi.org/10.1088/1748-9326/ab9467>.
- Yeom, J.-M., J.-L. Roujean, K.-S. Han, K.-S. Lee, and H.-W. Kim. 2020. "Thin Cloud Detection Over Land Using Background Surface Reflectance Based on the BRDF Model Applied to Geostationary Ocean Color Imager (GOCI) Satellite Data Sets." *Remote Sensing of Environment* 239:111610. <https://doi.org/10.1016/j.rse.2019.111610>.
- Ye, W., F. Zhang, and Z. Du. 2022. "Machine Learning in Extreme Value Analysis, an Approach to Detecting Harmful Algal Blooms with Long-Term Multisource Satellite Data." *Remote Sensing* 14 (16): 3918. <https://doi.org/10.3390/rs14163918>.
- Yong, S.-S., G.-S. Kang, S. Huh, and S.-Y. Cha. 2021. "Current Status and Results of In-Orbit Function, Radiometric Calibration and INR of GOCI-II (Geostationary Ocean Color Imager 2) on Geo-KOMPSAT-2B." *Korean Journal of Remote Sensing* 37 (5\_2): 1235–1243.
- Yoo, J.-M., G.-H. Choo, K.-H. Lee, D. L. Wu, J.-H. Yang, J.-D. Park, Y.-S. Choi, D.-B. Shin, J.-H. Jeong, and J.-M. Yoo. 2018. "Improved Detection of Low Stratus and Fog at Dawn from Dual Geostationary (COMS and FY-2D) Satellites." *Remote Sensing of Environment* 211:292–306. <https://doi.org/10.1016/j.rse.2018.04.019>.
- Yoon, J.-E., J.-H. Lim, S. Son, S.-H. Youn, H.-J. Oh, J.-D. Hwang, J.-I. Kwon, S.-S. Kim, and I.-N. Kim. 2019. "Assessment of Satellite-Based Chlorophyll-A Algorithms in Eutrophic Korean Coastal Waters: Jinhae Bay Case Study." *Frontiers in Marine Science* 6:6. <https://doi.org/10.3389/fmars.2019.00359>.
- Yu, X. L. 2013. 'Study on Retrieval of Sediment Concentration in Bo and Yellow Sea and Imputation of Missing Value Based on GOCI'. Master's Thesis, Qingdao, China: Ocean University of China.
- Yulong, G., H. Changchun, L. Yunmei, D. Chenggong, S. Lingfei, L. Yuan, C. Weiqiang, W. Hejie, C. Enxiang, and J. Guangxing. 2022. "Hyperspectral Reconstruction Method for Optically Complex Inland Waters Based on Bio-Optical Model and Sparse Representing." *Remote Sensing of Environment* 276:113045. <https://doi.org/10.1016/j.rse.2022.113045>.
- Zaneveld, J., and V. Ronald. 2013. "Fifty Years of Inherent Optical Properties." *Methods in Oceanography* 7:3–20. <https://doi.org/10.1016/j.mio.2014.03.002>.
- Zhang, Z., and Q. Du. 2022. "Hourly Mapping of Surface Air Temperature by Blending Geostationary Datasets from the Two-Satellite System of GOES-R Series." *Isprs Journal of Photogrammetry & Remote Sensing* 183:111–128. <https://doi.org/10.1016/j.isprsjprs.2021.10.022>.
- Zhang, X., Z. Jiao, C. Zhao, J. Guo, Z. Zhu, Z. Liu, Y. Dong, et al. 2022. "Evaluation of BRDF Information Retrieved from Time-Series Multiangle Data of the Himawari-8 AHI." *Remote Sensing* 14 (1): 139. <https://doi.org/10.3390/rs14010139>.
- Zhang, H., and M. Wang. 2010. "Evaluation of Sun Glint Models Using MODIS Measurements." *Journal of Quantitative Spectroscopy & Radiative Transfer* 111 (3): 492–506. <https://doi.org/10.1016/j.jqsrt.2009.10.001>.
- Zhang, F., N. Weng Chan, C. Liu, X. Wang, J. Shi, H.-T. Kung, X. Li, T. Guo, W. Wang, and N. Cao. 2021. "Water Quality Index (WQI) as a Potential Proxy for Remote Sensing Evaluation of Water Quality in Arid Areas." *Water* 13 (22): 3250. <https://doi.org/10.3390/w13223250>.
- Zhou, Y., D. Yu, W. Cheng, Y. Gai, H. Yao, L. Yang, and S. Pan. 2022. "Monitoring Multi-Temporal and Spatial Variations of Water Transparency in the Jiaozhou Bay Using GOCI Data." *Marine Pollution Bulletin* 180:113815. <https://doi.org/10.1016/j.marpolbul.2022.113815>.